

European Commission

# nuclear science and technology

## **Seismic Validation of 3-D Thermo-Mechanical Models for the Prediction of the Rock Damage around Radioactive Waste Packages in Geological Repositories**

### **SAFETI**

R.P. Young<sup>1</sup>, D.S. Collins<sup>1</sup>, J. Hazzard<sup>1</sup>, A. Heath<sup>1</sup>, W.S. Pettitt<sup>2</sup>, C. Baker<sup>2</sup>, D. Billaux<sup>3</sup>,  
P. Cundall<sup>3</sup>, D. Potyondy<sup>3</sup>, F. Dedecker<sup>3</sup>, C. Svemar<sup>4</sup>, P. Lebon<sup>5</sup>

<sup>1</sup>University of Liverpool (UK)

<sup>2</sup>Applied Seismology Consultants — ASC Ltd (UK)

<sup>3</sup>ITASCA Consultants SA (FR)

<sup>4</sup>Svensk Kärnbränslehantering — SKB AB (SE)

<sup>5</sup>Agence nationale pour la gestion des déchets radioactifs — ANDRA (FR)

Contract N° FIKW-CT-2001-00200

### **Final report**

Work performed as part of the European Atomic Energy Community's R&T Specific Programme  
“Nuclear Energy, Key Action: Nuclear Fission Safety 1998-2002”  
Area: Safety of the Fuel Cycle

Directorate-General for Research  
Euratom

2005

EUR 21925

## EXECUTIVE SUMMARY

Until now, computational limitations have meant that it was not practical to produce detailed three-dimensional (3D) field-scale experiments using discrete element modelling codes. The SAFETI project has produced a state of the art code (AC/DC) and visualization package (ACDCvis) that allows models of field-scale experiments in brittle materials (such as rock or concrete) to be performed. The code makes use of parallel computing technology, and has been successfully tested on 40 nodes of the Networked Earth Science Super Computer (NESSC) at Liverpool University, and a smaller computer cluster in France.

The models can contain excavations and an in-situ 3D stress field can be applied. Microcracking is interpreted at the regions in the model where bond breakages occur between the model particles. The microcracks can be viewed and analyzed in terms of their location, orientation, and basic failure mechanism (shear or tensile). Further algorithms have been developed for spatially and temporally interpreting the microcracks in terms of acoustic emission/microseismic (AE/MS) parameters including magnitude and the moment tensor source mechanism. Methods for measuring the static and dynamic stiffness tensor at specific locations within a 3D AC/DC model have been developed, which allows the damage and anisotropy to be quantified. Algorithms have been produced for predicting time dependent behaviour in the AC/DC model, calibrated to laboratory measurements. Methods have also been developed for interpreting and visualizing (using 3FLO) the hydraulic fracture network, and calculating the corresponding hydraulic parameters.

The starting point for AC/DC was the well known and accepted PFC3D (discontinuum) and FLAC3D (continuum) codes. The AC/DC concept uses a building block called a periodic cell or 'pbrick'. Pbricks are built from spherical particles of specific stiffnesses and bond strengths using a calibrated method. The method requires that standard rock test parameters are known, including Young's modulus, Poisson's ratio, crack-initiation stress and uniaxial compressive strength (UCS).

Pbricks are made in a way that allows them to fit perfectly together in 3D to allow large models to be constructed. Three types of pbrick were developed. The particle pbrick is a densely packed assembly of PFC3D particles at equilibrium. The matrix pbrick is a more computationally efficient version of the particle pbrick in which cracking can not occur. The degenerate matrix pbrick is a FLAC3D zone, and is a more computationally efficient version of the matrix pbrick. Degenerate matrix pbricks are generally useful on the outer portions of models to gain the correct boundary and stress conditions. Adaptive logic was written to convert matrix pbricks to particle pbricks as required near regions of new bond-breakages (microcracking), automatically as the model runs.

Well controlled polyaxial laboratory experiments were performed on Crosland Hill sandstone at Imperial College London, to provide AE and modulus validation data. PFC3D and AC/DC models were performed of these experiments with the models showing a number of similarities to the measured behaviour. Data from SKB's prototype repository test (PRT) was analyzed in terms of AE and modulus variation. In this experiment a field scale deposition hole was excavated at 440m depth in Aspo diorite in Sweden. Multi-million particle AC/DC models were performed of this excavation, with the modelled and measured data showing similarities in their spatial distribution and source mechanism. AC/DC models were also produced of excavations in Bure Callovo-Oxfordian argillite and Mont Terri Opalinus clay. Using calibrated long-term algorithms, the stress induced microcracking over a 2 year period was analyzed around both excavations. Additionally the hydraulic fracture network and associated hydraulic parameters were determined.

The primary aim of AC/DC is as a tool for nuclear repository development programs. At the early stages of site selection and characterization, the code provides a method for predicting the microcrack response of different rock types to excavation and stress. For repository layout design, AC/DC provides a method for analyzing the excavation damage zone (EDZ) development from

different deposition hole spacing. AC/DC is also of interest to a larger geoscience and engineering sector. The AC/DC methodology can be applied for example, to concrete structures such as dams, particularly for understanding their long-term stability due to material degradation. AC/DC is of interest to petroleum companies to model the effect of reservoir property change with time, and to mining companies in terms of gallery excavation and safety. AC/DC is also an important research tool for Earth Science departments and large geological organisations.

# TABLE OF CONTENTS

<b>EXECUTIVE SUMMARY .....</b>	<b>III</b>
<b>1 INTRODUCTION AND OBJECTIVES .....</b>	<b>1</b>
<b>2 SCIENTIFIC AND TECHNICAL DESCRIPTION OF THE RESULTS .....</b>	<b>3</b>
2.1 AC/DC Modelling Software .....	3
2.2 Visualization Software .....	5
2.3 Procedures for Modelling Rock.....	6
2.3.1 Producing a ‘Model of Rock’ .....	6
2.3.1.1 PFC3D.....	6
2.3.1.2 AC/DC.....	6
2.3.2 Predicting Long Term Effects .....	7
2.3.2.1 Stress Corrosion Method Applied to Granite/Diorite .....	7
2.3.2.2 Micro Constitutive Law for Clay .....	8
2.3.3 Measuring the Static Elastic Constants .....	8
2.4 Algorithms for Seismic Modelling of Rock.....	9
2.4.1 Calculating Seismic Source Parameters .....	9
2.4.2 Velocity Interferometry and Determining Dynamic Elastic Constants .....	11
2.5 Laboratory Seismic Data Set .....	13
2.6 Excavation Scale Seismic Data Set .....	17
2.7 Modelling the Hydraulic Fracture Network.....	20
2.8 Modelled Results and Comparison with Measured Data.....	21
2.8.1 Laboratory .....	21
2.8.1.1 Crosland Hill Sandstone Polyaxial Test .....	21
2.8.1.2 SKB Äspö Diorite .....	24
2.8.1.3 Mont Terri Opalinus Clay Rock .....	24
2.8.1.4 Bure Callovo-Oxfordian Argillite .....	26
2.8.2 Excavation Scale .....	27
2.8.2.1 SKB Diorite Prototype Repository Test .....	27
2.8.2.2 Mont Terri Clay Excavation.....	30
2.8.2.3 Bure Argillite Prediction .....	32
<b>3 ASSESSMENT OF RESULTS AND CONCLUSIONS .....</b>	<b>34</b>
<b>4 ACKNOWLEDGEMENTS .....</b>	<b>36</b>
<b>5 REFERENCES .....</b>	<b>36</b>
<b>6 GLOSSARY .....</b>	<b>37</b>
<b>7 APPENDIX 1 - LIST OF DELIVERABLES .....</b>	<b>38</b>
<b>8 APPENDIX 2 – EXPLOITATION AND DISSEMINATION .....</b>	<b>39</b>
<b>9 APPENDIX 3 – CONTACT DETAILS CONCERNING FOLLOW-UP OF THE PROJECT.....</b>	<b>42</b>

# 1 INTRODUCTION AND OBJECTIVES

In order to study the concepts and issues relating to nuclear waste repository engineering, a number of sub-surface test facilities have been constructed world-wide and several others are planned or already under construction. These facilities are providing important opportunities to develop methodologies and techniques that could ultimately be used for repository engineering. One of the key questions that must be addressed when considering the technical feasibility of geological disposal is the short- and long-term response of the rock mass. This involves times well beyond the range of consideration in classical rock engineering projects.

The major objective of this project was to develop a systematic approach to understanding such rock mass behaviour by integrating observational and numerical methods to realistic 3D models of repository excavations. The application of numerical modelling to repository simulations has been restricted to either rather simplistic models that do not account for the detailed response of the rock with time or more complex models that simulate the details of the rock mass response, but which are restricted to small scales or 2D cases. The ability to simulate the long-term behaviour of a rock mass is very important for repository engineering, since the operational life of this type of facility is in excess of almost any other structure engineered by mankind.

Traditionally, the application of numerical models to engineering has made use of continuum codes. These are ideal for situations where the failure occurs primarily due to tensile stresses, as once failure has occurred there is no interaction between the failure surfaces. However, in rock engineering problems, where the applied loads are essentially compressive (gravitational & tectonic) then rupture surfaces continue to interact after failure. A discontinuum particle model is then needed to model the complex features of the disintegration process. Discontinuum codes, that simulate rock as an assembly of distinct elements or particles, have already shown considerable promise in reproducing the mechanics of rock failure. In particular PFC (Particle Flow Code), produced by the Itasca Consulting Group, has been shown to reproduce both static and dynamic elements of rock behaviour (Potyondy et al. 1996; Potyondy and Cundall 1998 & 1999 & 2001). AE/MS (acoustic emission/microseismic) data contains information on the actual three-dimensional damage process and is therefore ideal for model validation (Hazzard et al. 2000).

In the past, computational limitations have meant it was unfeasible to produce detailed field-scale models using discrete element codes. This project was feasible because of two developments. The first development was that one of the consortium members (Liverpool University) was awarded access to a massively parallelised supercomputer (NESSC). Secondly, the consortium members conceived a coupled, 3D, modelling approach partially based upon the codes PFC3D and FLAC3D. The scheme is named AC/DC (Adaptive Continuum/DisContinuum).

In summary, the main scientific/technological objectives of the project were:

- Produce the AC/DC code and install on a parallel supercomputer cluster running under Linux.
- Produce a visualization package, to allow users to remotely analyze the AC/DC model and compare with measured data.
- Develop procedures for producing PFC3D and AC/DC 'Models of Rock', utilizing the sensitivity of the model microparameters to the overall macro-behaviour.
- Develop algorithms for analyzing PFC3D and AC/DC 'Models of Rock', including static and dynamic elastic modulus in 3D, and AE/MS activity.
- Develop algorithms that mimic the long-term damage processes in rock.
- Produce measured datasets from laboratory rock tests and field scale excavation experiments, that can be used for model validation.
- Produce models with PFC3D and AC/DC utilizing the short and long-term algorithms and compare to the measured datasets. Perform extensive testing to validate the behaviour of the PFC3D and AC/DC approach.

- Develop algorithms to describe the time dependent microfracturing in specific soft rocks, namely Bure Callovo-Oxfordian argillite and Mont Terri Opalinus clay rock.
- Develop a method for interpreting and visualizing the hydraulic fracture network, and calculating the corresponding hydraulic parameters.
- Produce a PFC3D 'Model of Rock' for both the argillite and clay rock.
- Produce a field scale AC/DC model of an excavation in argillite and clay rock.
- Determine the fracture network and corresponding hydraulic parameters for both field-scale models

## 2 SCIENTIFIC AND TECHNICAL DESCRIPTION OF THE RESULTS

### 2.1 AC/DC MODELLING SOFTWARE

The project has developed and tested a modelling software package called AC/DC. The package builds on the existing Particle Flow Code (PFC) to provide new parallel and adaptive capabilities. The software allows a 3D particle model to be split, in an arbitrary way, between multiple processors. Further, remote regions may be represented by the matrix equivalents of continuum elements, which are replaced as the model is running by particles, under control of an adaptive algorithm, which ensures that the particle representation exists in a region before cracks reach that region.

The basic building block for AC/DC is the periodic cell, known as the ‘p-cell’ or ‘pbrick’. The pbrick concept allows large models to be quickly built up, as well as allowing the model to be easily divided between parallelised processors. There are three types of pbrick:

1. Particle Pbrick: A densely packed assembly of PFC3D particles at equilibrium.
2. Matrix Pbrick: A particle pbrick in which the particles are replaced with a matrix. The matrix is essentially a network of masses and springs (i.e. no rotation can occur and no formation or loss of contacts).
3. Degenerate Matrix Pbrick: A particle pbrick in which the particles are replaced by a continuum FLAC3D zone. This is a more simple version of the matrix pbrick.

An example of a particle pbrick is shown in Figure 1a. An example of the ‘repeating boundaries’ of pbricks is shown in Figure 1b, where 3 pbricks are connected together, to form a larger model.

The matrix pbrick is a reasonable assumption in regions where microcracking is not expected, and also makes the model much more computationally efficient. Degenerate matrix pbricks are even more computationally efficient than matrix pbricks, and are useful to use on the outer portions of large models to gain the correct boundary and stress conditions.

Adaptive logic has been written to convert matrix pbricks to particle pbricks as required near regions of new bond-breakages (microcracking). Figure 2 presents two time steps from a simple AC/DC model made of 36 pbricks. Following the creation of new microcracks the model is seen to convert a number of the matrix pbricks into particle pbricks.

More details of the achievements of the codes are as follows:

- A kernel version of PFC (both 2D and 3D) runs under Linux on the parallel computer cluster, NESSC. An optional PFC mode allows commands directed to the root process of PFC to be passed automatically to all other PFC processes; thus any number of parallel invocations of PFC can be run in step.
- PFC contains a communications thread that accepts requests from ACDCvis, and supplies it with the appropriate data for display. The requests are processed at any time while PFC is running, and can come from any remote machine (on a LAN, or on the Internet).
- Particle assemblies may be created within a rectangular periodic space. A compacted and equilibrated assembly thus created may be stored in compact form, and invoked whenever it is needed, to create larger composite assemblies.
- Two modes of creating large assemblies exist. First, any number of pbricks may be attached directly. The resulting assembly behaves in exactly the same way as a regular PFC assembly. Second, any number of pbricks may be created in contiguous regions of space, but not attached directly. In this case, known as multi mode, the attachment is via a buffer scheme, which passes messages, containing velocities and forces, between neighbouring pbrick boundaries. Both

generation schemes guarantee equilibrium of the resulting assembly, and mechanical behaviour is identical.

- In multi mode, the pbricks that comprise the assembly may be distributed in any way between parallel instances of PFC, including the limiting case of a single process. For adjacent bricks that exist on separate processes, the messages described above are passed with MPI (Message Passing Interface) functions; otherwise, messages are passed via a local buffer. The multiple-processor version of PFC may be run on a Microsoft Windows platform, as well as Linux.
- A simplified matrix equivalent to the particle pbrick may be substituted for any brick in an assembly, giving more rapid calculation speed compared to a pbrick containing regular particles. The facility also exists to substitute a “degenerate” matrix for any pbrick, which is the equivalent of an 8-node elastic element in 3D and a 4-node element in 2D. Both matrix forms may be regarded as equivalent continuum elements
- Functionality exists in PFC to support matrix/continuum pbricks, such as plot items, fix/free commands and initial velocity commands. The support for deletion within regions of space (e.g., to construct a tunnel) is aware of multi mode, so that the message-passing logic recognizes that certain particles may not exist.
- A FISH (Itasca programming language) function exists to extract a 3D degenerate matrix pbrick from a continuum, elastic brick, modelled with the program FLAC3D.
- Substitutions between the various forms of pbricks that comprise a complete assembly may be made at any time and at any location during a simulation. In particular, the particle form may be substituted for the matrix form, when control logic detects that cracks are approaching a region that contains an elastic, continuum representation. Thus, particles are installed in a region before nonlinear mechanisms occur in the region. The strains within a deformed matrix brick are used to estimate contact forces, when the brick is replaced by a particle form.

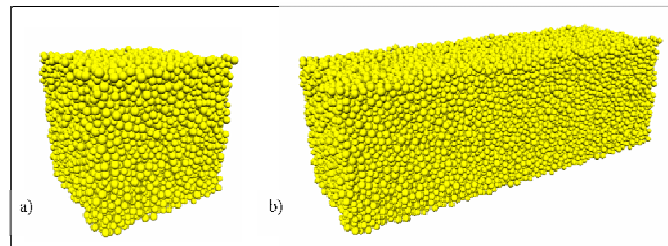


**Figure 1: Examples of (a) a particle periodic cell (pbrick), and (b) an assembly of three particle pbricks.**

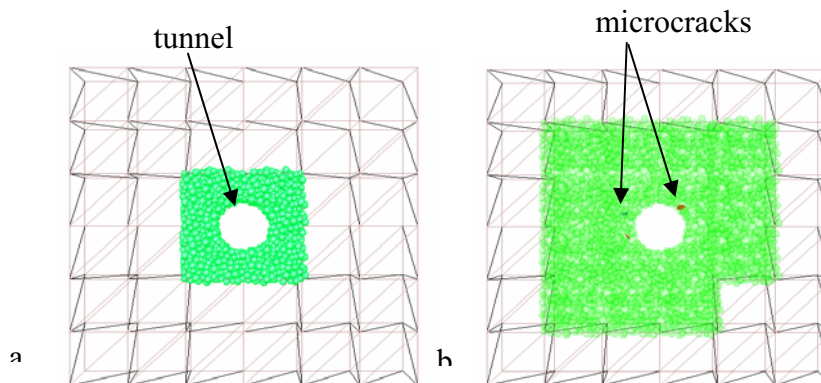


**Figure 2: An AC/DC model made of a combination of 32 full-matrix pbricks and 4 particle pbricks. A tunnel has been created in the center of the sample. b) The same AC/DC model following the creation of stress induced bond-breakages interpreted to be microcracking. The adaptive logic incorporated into the AC/DC model has converted a number of the full-matrix pbricks into particle pbricks near the regions of microcracking.**



## 2.2 VISUALIZATION SOFTWARE

A visualization program, 'ACDCvis', has been produced and tested. ACDCvis is a program for displaying model and experimental data. 'Objects' (e.g. model balls, model cracks, seismic events, seismic source mechanisms, etc) can be displayed in 3D, with options to scale by size or colour to relevant 'parameters' (e.g. ball radius, crack type, event magnitude, event location error, etc). A graphical shape is associated with each object (e.g. sphere, vector, disc, ellipsoid, etc) and can be displayed as wire-frame or shaded and with or without a light source effect. Additionally AutoCAD DXF files and INSITE DOF files can be displayed, allowing 3D lines, triangles, and planes to be visualized. ACDCvis allows the user to perform various analysis techniques including: 3D rotation, translation, zoom, turning the display of an object on or off, varying the object opacity, setting an object to be single coloured or colour graded to a parameter, and setting an object to be single sized or size scaled to a parameter. Clipping planes (parallel to the three principal axes) can be moved to allow slices through the 3D volume to be viewed. All objects have a time associated with them, and a VCR mode allows the data to be displayed in user defined time steps forwards or backwards. A cumulative option is also available.

A special file format (VVF) has been developed to allow the exchange of information between AC/DC (and PFC3D), ACDCvis and other programs. This dynamic file type can have a number of different columns of data (user set) including model and experimental objects and parameters. FISH functions have been written to convert PFC3D data into VVF. AC/DC produces VVF's while it is running after a certain number of user-defined time steps. ASC's seismic processing software (INSITE) also exports VVF data.

ACDCvis runs on either a computer with a Windows operating system, or with a 'Windows Emulator' (e.g. WINE) from an operating system such as Linux. Figure 3 is a screen capture from ACDCvis, showing examples of model data and the display functions.

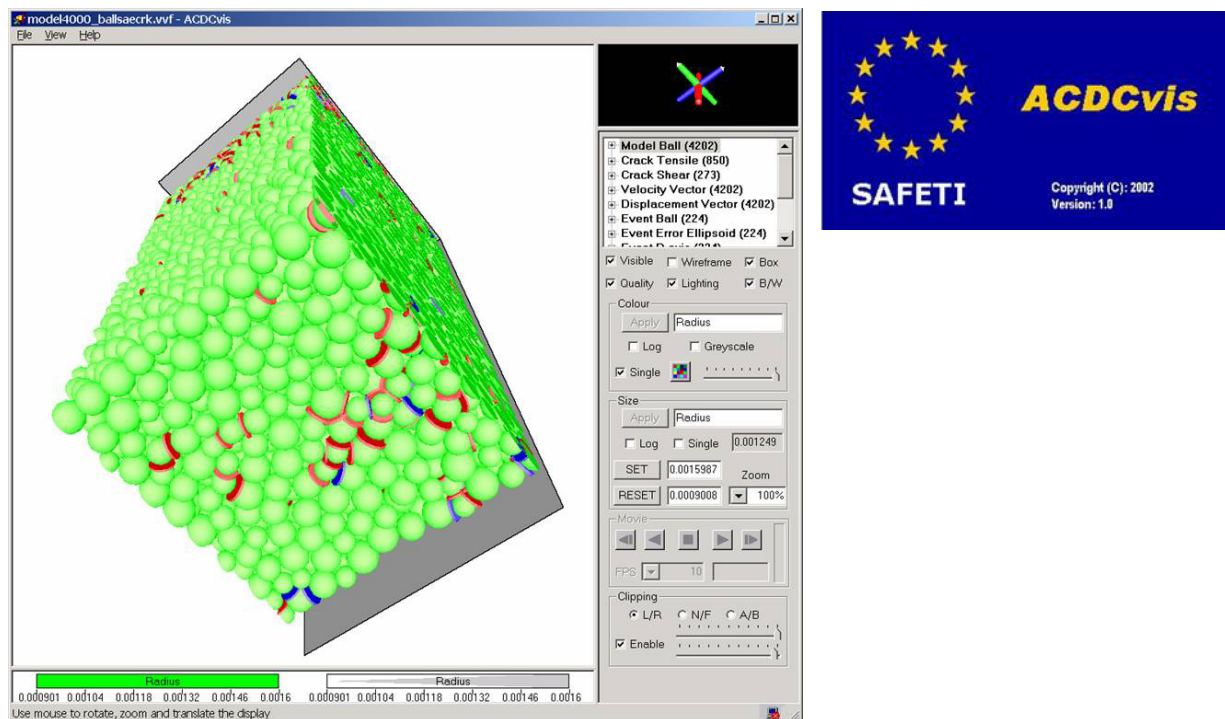


**Figure 3: An example of ACDCvis, showing a cutting plane through a model of granite, showing the particles in green, as well as tensile bond breaks (microcracks) in red, and shear microcracks in blue.**

## 2.3 PROCEDURES FOR MODELLING ROCK

### 2.3.1 Producing a ‘Model of Rock’

#### 2.3.1.1 PFC3D

A well-defined procedure has been developed to create a PFC3D material (Model of Rock) that exhibits a similar behaviour to the short term macroproperties of rock. The macroproperties include the Young’s modulus, Poisson’s ratio, crack-initiation stress and peak strength. These can be measured using a standard uniaxial strength test on the rock of interest. The measured macroproperties are compared to those from a uniaxial strength test simulation on the PFC3D material. The microproperties (particle and bond properties) are varied such that a best fit is found to the macro-behaviour.

The method was first tested and performed successfully for Lac du Bonnet granite. A study was also performed on the effect of particle size on the material macroproperties.

The effect of a boundary layer in PFC3D models was also investigated. A boundary layer forms in the model when the particles next to confining walls are preferentially aligned. Figure 4 shows examples of two cylindrical samples prepared for a uniaxial strength test simulation, with one having aligned particles along the boundary, and one with non-aligned particles. The sample with non-aligned particles was found to be more representative of a homogeneous material.

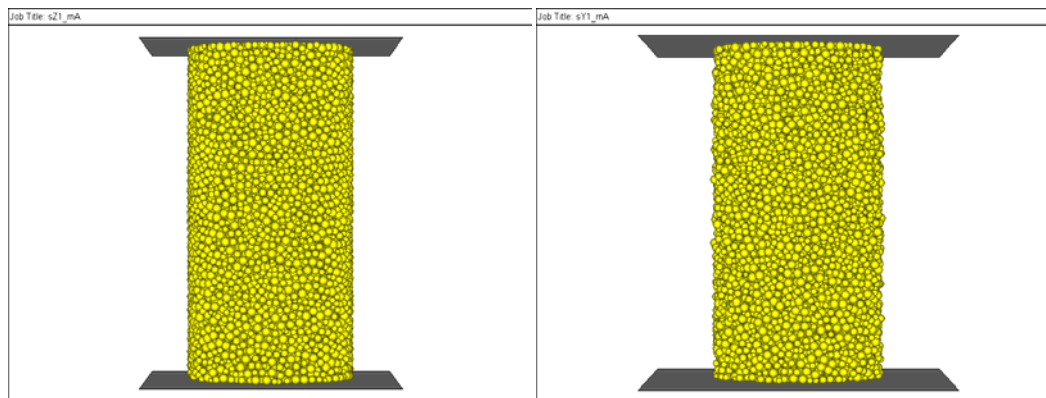


**Figure 4: Examples of the preparation of cylindrical specimens of PFC3D material for uniaxial strength testing. The sample on the left has aligned particles along the boundaries, whereas the sample on the right does not. It was concluded that the sample on the right is more representative of real rock.**

#### 2.3.1.2 AC/DC

A well defined procedure now exists for creating AC/DC models. Algorithms were developed to:

- Construct a PFC3D ‘Model of Rock’ in periodic space.
- Use this material as a periodic brick (pbrick) to produce an AC/DC model of the region of interest.
- Install a uniform in-situ stress field.
- Simulate an excavation by removing particles in the region of interest.
- Monitor and output deformation and damage.

Two methods for installing an initial stress state have been investigated. The first one, replicates the pbrick before installing the initial stress state in the entire model. The second one

installs the initial stress state on the pbrick before replicating it. This latter method is found to produce equivalent results to the first method, but is significantly more efficient.

An assessment of the accuracy of the AC/DC formulation (wherein matrix pbricks are substituted for particle pbricks in the region remote from the active damage zone) has been performed by comparing the stress and deformation fields surrounding an excavation in an elastic body with the Kirsch solution. Four different sample constructions were tested, each one moving closer to a full AC/DC model simulation. The models show good agreement between the theoretical and numerical displacement field, indicating the different pbrick types are working correctly together.

### 2.3.2 Predicting Long Term Effects

#### 2.3.2.1 Stress Corrosion Method Applied to Granite/Diorite

The PFC3D model has been enhanced to include time-dependent behaviour by adding a micro-damage process based on a stress-corrosion mechanism. Long-term damage has been observed in a number of hard-rock studies as the slow growth of numerous microcracks (e.g. Young et al 2004, Kranz and Estey, 1996). The model represents this long-term damage process.

The model has three main parameters that control the removal of bonding material at a certain rate at each parallel bond that is loaded above its micro-activation stress. This produces a stiffness reduction and a stress increase in the remaining bond material, which fails when the stress being carried exceeds the bond strength. Chemical reaction rate theory is used to obtain the proper parameterization and stress dependence of the corrosive front velocity. The three parameters can be calibrated by matching (1) the time-to-failure curve produced by performing a series of static-fatigue tests, (2) the loading-rate dependence of compression strengths, or (3) the velocity versus stress-intensity factor curve of a single macroscopic fracture subjected to pure mode I tension. Only the first calibration procedure has been performed to date.

Figure 5 presents results for the model calibration of Lac du Bonnet granite. The time to failure is plotted versus the failure strength normalized to the short term strength, for both the model and measured laboratory data. A reasonable match of the PFC material to the measured results is found. The long term strength values of the PFC material are also found to be relatively independent of particle size (as shown by the models with different 'res' values).

The model has been implemented for PFC3D and AC/DC, and builds on an earlier implementation that was only for PFC2D. FISH functions have been developed to support static-fatigue testing of the PFC3D material.

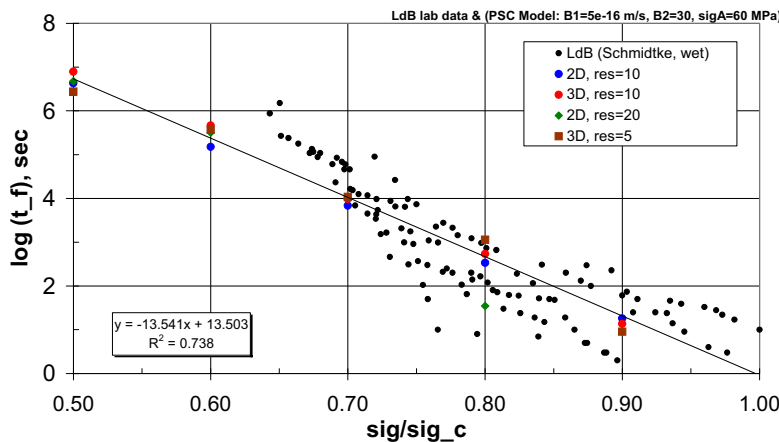


**Figure 5: Static-fatigue curve for PFC granite material and Lac du Bonnet granite. Time to failure ( $t_f$ ) is plotted versus the failure strength ( $\text{sig}$ ) normalized by the short term failure strength ( $\text{sig}_c$ ). The variable 'res' refers to models with different ranges of particle sizes.**

### 2.3.2.2 Micro Constitutive Law for Clay

Creep is a time dependent deformation process occurring on the microscopic scale of clay. Microscopic bonds, such as Van-der-Waals forces, liquid bridges, crystal bridges break during a small deformation under load. Simultaneously, new microscopic bonds emerge when new particle pairs come into contact. Dependent on the ratio of breaking and emerging bonds the number of total bonds can increase or decrease. This effect has been used for the implementation of the creep mechanism in the PFC3D model. The number of microscopic bonds is related to the thickness of the mesoscopic parallel bonds and the velocity at which the bonds change their thickness is controlled by the creep law. The creep law takes into account the fact that the shear stress in a parallel bond is a measure of the shear deformation.

Three slightly different equations for the shrinkage velocity  $v_{\text{shrink}}$  of parallel bonds have been tested: an exponential law, a power law and a trigonometric law. Taking into account the results (Figure 6), the power law was chosen as the best one. The model has been implemented for PFC3D, and FISH functions have been developed.

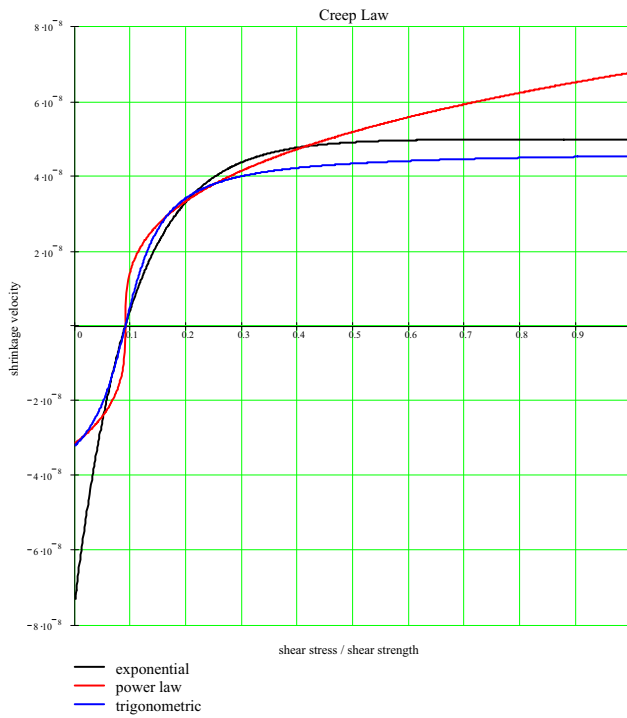


Figure 6: Graphs of the shrinkage velocity according to the three creep laws tested.

### 2.3.3 Measuring the Static Elastic Constants

A PFC3D stiffness probe method (Method SP) has been developed to measure the 36 independent components of the stiffness tensor of a PFC3D material. It does this by taking a spherical region (Figure 7) and applying strain perturbations and measuring the induced stress perturbations. The components of the stiffness tensor are defined as  $c_{qr}$  ( $q, r = 1$  to 6). The stiffness can be measured at any stage of a PFC3D simulation, and can also be used in AC/DC field-scale models.

A second method has been developed for measuring static elastic constants. This method is specific for cubic rock models in which stress is varied in three principal directions. Thus it mimics the polyaxial cell experiment performed at Imperial College, England, where the laboratory seismic

data set was collected. The polyaxial cell stress probe method (Method PS) measures nine of the 36 elastic compliances (which can be converted to a stiffness tensor) by performed three stress-strain excursions.

Both Methods PS and SP can be used assuming more simple symmetry systems, such as a transversely isotropic material. Error indices to quantify the goodness of fit of the material response to a particular material symmetry were also developed.

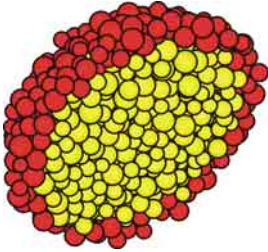


Figure 7: A cut-away view of a spherical core showing the concept of the PFC3D elastic-stiffness probe.

## 2.4 ALGORITHMS FOR SEISMIC MODELLING OF ROCK

### 2.4.1 *Calculating Seismic Source Parameters*

Algorithms for obtaining seismic source information in PFC3D and AC/DC models have been written and tested. Four main algorithms have been produced.

The first algorithm allows models to be run with realistic levels of seismic attenuation. A relationship has been derived that allows an amount of attenuation to be achieved by specifying the numerical damping in the model.

The second is a method for interpreting seismic events from bond breakages in the model. Each bond breakage is defined as a crack, and this was initially considered to also be a seismic event. However this was found to result in all of the events having a similar size and magnitude which is an uncommon situation in nature. Large seismic events in nature are generally made up of many smaller scale ruptures and shearing of asperities (Scholz, 1990). Additionally fractures are considered to grow at a finite velocity proportional to the shear wave velocity (Madariaga, 1976). Therefore, in the model, bond breakages occurring close in space and time are considered part of the same macro-rupturing event. If a new crack forms within the source area of an ‘active’ crack, then the two cracks are considered part of the same seismic event and the source area is expanded to encompass all of the source particles. Figure 8 shows an example of this in a model where three bond breakages occur quickly in time, and are all considered associated with the same active crack formation.

The third is the formulation of the moment tensor (MT). The MT is a representation of a seismic source by a set of equivalent forces that produce the same displacements throughout the rock as the actual forces at the source. It is a method used in all scales of seismic monitoring from laboratory studies to earthquake analysis, to interpret the source mechanism. MTs are plotted as 3 sets of perpendicular vectors indicating the maximum force directions and magnitudes at the source. In PFC3D, a surface around the source is defined by the contacts between the source particles and their neighbours. After a bond breaks, the MT for the event is calculated by summing the different components of moments at the contacts surrounding the source. Each moment at a contact is the change in contact force multiplied by the distance between the contact point and the event centroid. Figure 9 provides an example for a single tensile bond breakage. The 3 MTs presented in Figure 8 show how the time evolution of source mechanisms can be investigated in great detail using this modelling method.



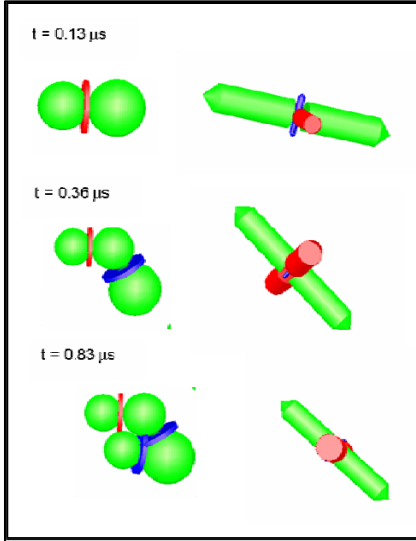


Figure 8: An example AE composed of 3 microcracks and its evolution through time. The left plot in each time frame shows source particles and cracks. The right plots show the calculated moment tensor. The pointed direction of the vectors shown in the moment tensor display, indicate the direction of tension or compression that is acting.

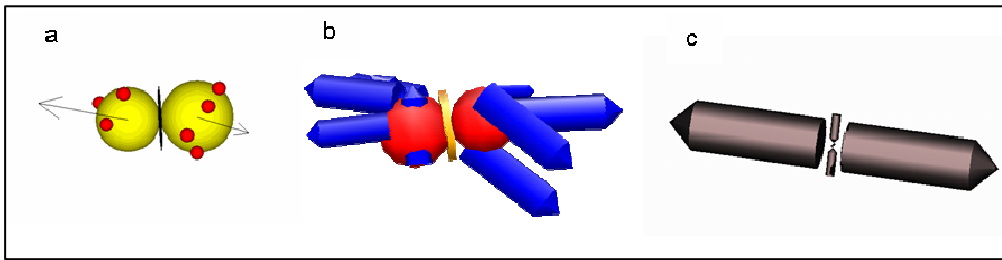


Figure 9: An example AE composed of a single tensile bond breakage. a) The two source particles and their displacements. The black disk represents the microcrack. The small red circles show the locations of contacts with surrounding particles. The displacement vectors are projections onto the 2D plotting plane. b) The force changes at the contacts during the event. c) The calculated moment tensor plotted as equivalent forces at the event centroid.

The fourth algorithm is the estimate of the event moment magnitude from the moment tensor. The scalar moment is calculated from the elements of the MT matrix. The moment magnitude is then calculated from the scalar moment using the relationship of Hanks and Kanamori (1979).

A first test of the algorithms was performed by simulating a generic 3D axial compression test on a core sample of Lac du Bonnet granite with 10MPa confinement. The PFC3D ‘Model of rock’ for this granite, developed as part of SAFETI, was used. The granite model was loaded to failure and 3041 seismic events were recorded. Due to the scale of the laboratory test, the seismic events are defined as acoustic emissions (AE). The AE locations and magnitudes before and after the peak stress were analysed. It was seen that before the peak stress, the events were randomly located throughout the sample with the largest events occurring at the top and bottom platens. After the peak stress there was a clear localisation and the AE lined up along two conjugate planes inclined at an angle to the maximum stress  $\sigma_1$ . This type of behaviour agreed with many other laboratory studies that show sample failure along inclined shear planes in confined loading tests (Jaeger and Cook, 1969). In addition, the moment magnitudes of the events (-7.6 to -4.1) seemed realistic for this type of test. The MTs showed the direction of maximum pressure for most events to be sub-vertical, and therefore sub-parallel to the maximum stress direction. The direction of maximum tension was generally sub-horizontal. The large tensile forces at many of the sources

indicated tensile cracks opening perpendicular to the  $\sigma_1$ . This prevalence of sub-vertical tensile cracking agreed with other laboratory studies (Lei et al. 2000) and with physical observations (Tapponnier and Brace 1976; Moore and Lockner 1995).

The algorithms were adapted to work for parallel processing (AC/DC). As a test of the parallel node communication, two models of identical particle size and shape were created. The first model was created with PFC3D and run on one node of NESSC. The second model was made of three particle pbricks in AC/DC and run on three nodes of NESSC. Both models experienced the same compressive load history, which produced a strain in the long direction of approximately 1.5%. The induced microcracking was interpreted as seismic events using the clustering (space and time) algorithm. These seismic events are shown for both models in Figure 10. The results are virtually identical, indicating that AC/DC can be used to successfully produce these type of models. The very slight differences in Figure 10 occur because the seismic activity in AC/DC is interpreted independently on each parallel node. Therefore in the clustering algorithm, events can not propagate between nodes. This issue will be considered in future versions of AC/DC, but the code modifications were considered too complex to perform for this study. However, it is thought that the scenario of seismic events propagating across nodes will be fairly rare, and therefore the error produced by not considering this effect will be minor. For example, occasionally the difference may be 2 smaller events in AC/DC compared to 1 larger event in PFC3D.

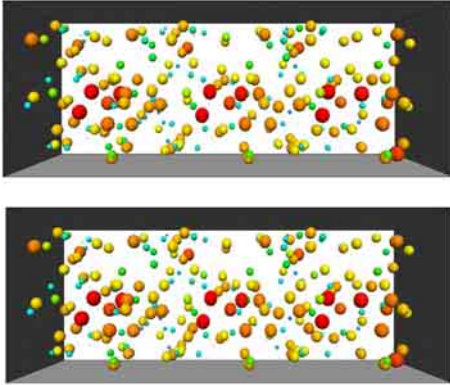


**Figure 10: Seismic events interpreted in two models that have experienced the same stress history. The top model is a single PFC3D model running on a single node. The bottom model is an AC/DC model made of 3 particle pbricks (Figure 1b) with each pbrick running on a different node of the super computer. The events are coloured and scale to relativemagnitude.**

#### ***2.4.2 Velocity Interferometry and Determining Dynamic Elastic Constants***

A methodology has been developed to propagate p- and s-waves across PFC3D and AC/DC models. The measured waveforms can be interpreted using seismic processing methods to determine p- and s-wave velocities and these results can be further interpreted in terms of dynamic moduli and crack density parameters. This was termed the wave-velocity probe method (Method WV).

The important issue of dispersion was considered. Non-continuum materials (real and numerical) will experience wave dispersion if the wavelength of the propagating wave approaches the size of the individual elements. Kuhlemeyer and Lysmer (1973) show that waves cannot propagate if there are less than 4 elements per wavelength and that significant errors are introduced if there are less than 10 elements per wavelength. Dispersion error also increases with distance of wave propagation, therefore the choice of wavelength must also consider the size of the sample. In the algorithm developed, wave frequencies were assigned such that there were approximately 15 particles per wavelength.

The density of the particles in a PFC3D model has no effect on the model behaviour when run in pseudo-static mode (high damping). However, the density does effect the speed of wave propagation when run dynamically (low damping). To obtain realistic wave velocities, it was found that the densities of the particles must be set such that the overall density of the sample (particles plus voids) is equal to the desired density. Particle densities must therefore be calculated by taking into account the porosity  $\phi$  of the PFC3D model.

The velocity measurement involves choosing a particle as a transmitter, and a second particle at some distance as a receiver. A Ricker wavelet with a user set dominant frequency was specified to be the velocity of the transmitter. This type of wavelet was chosen because it has no high frequency corners, thereby minimising dispersion. An example of wave propagation is shown in Figure 11, where a p-wave source is propagated from left to right through a cubic PFC3D model. The method involves taking the recorded waveforms and inputting them into INSITE for seismic interpretation. Elastic stiffness values can then be determined by for instance assuming an isotropic or transversely isotropic material.

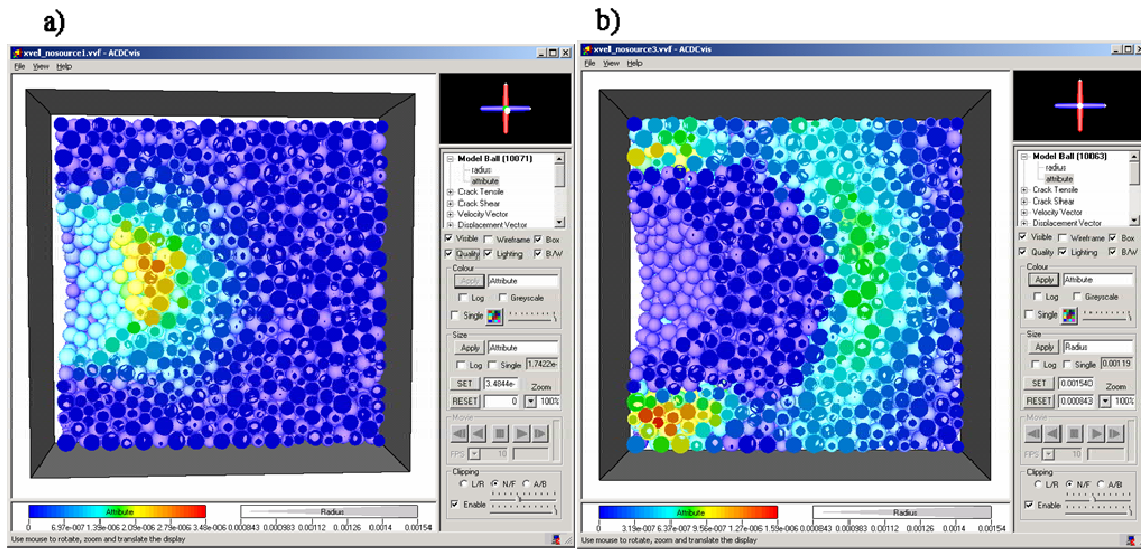


**Figure 11: An example of the wave propagation through a particle pbrick model is shown, with (a) being an earlier time step than (b). This example shows a P-wave Ricker wavelet source starting from the left side of the model. The particle velocity is shown as a normalized magnitude between blue and red.**

The wave propagation algorithms were implemented into AC/DC, and tested. The first test consisted of creating two models of identical particle size and shape. The first model was created with PFC3D and run on one node of NESSC. The second model was made of three particle pbricks in AC/DC and run on three nodes of NESSC. A third model was also created, similar to the second model, but with the central particle pbrick changed to a matrix pbrick. Figure 12 shows the setup of the model and transmitter and receiver locations. Summary results from this test are presented in Table 1. The solution for Models 1 and 2 is the same within 0.1%, indicating the successful implementation of the velocity modelling in AC/DC. However, the results for Model 3 which contains a matrix pbrick, is almost two orders of magnitude lower than in the other models, and the wave arrives later. The reason for this is that the matrix pbrick is fully damped throughout the test. This issue is not believed to be a major problem since the major regions of interest for velocity measurements are through areas where microcracking is occurring, which are always particle pbricks. Allowing velocity measurements through both particle and matrix pbricks will be considered in future versions of AC/DC.



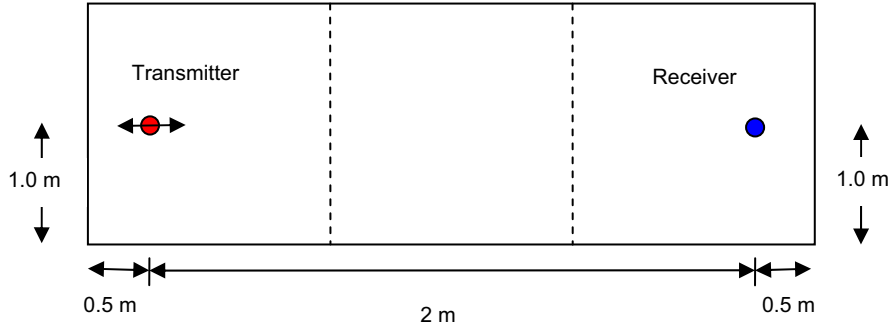


**Figure 12: Side view of the model geometry for testing wave propagation in AC/DC. The dotted lines indicate internal boundaries between pbricks (each 2 m cubes). The model extends 2 m into the page, therefore the top view looks the same. The arrows superimposed on the transmitter show the direction of applied particle velocity.**

Model	Wave velocity (m/s)	First peak amplitude ( $\infty$ m/s)
1	6303	5.446
2	6295	5.446
3	5528	0.0670

**Table 1: Results of wave propagation test.**

## 2.5 LABORATORY SEISMIC DATA SET

The primary objective was to produce a laboratory seismic data set that could be used to validate results from PFC3D models. The types of data that were required included static and dynamic elastic constants in different directions, and AE data. Following initial discussions, it was chosen to use a true-triaxial (polyaxial) cell at Imperial College in London, in which stresses can be independently applied in the three principal directions.

A load history was chosen which should conceptually induce a set of aligned microcracks through the sample. Figure 13 shows a schematic diagram of the idealized cube rock sample, and the types of measurements to be performed. One limitation was that the polyaxial equipment could not apply enough stress to break high strength granitic rocks. Therefore the rock sample was chosen to be the medium strength Crosland Hill sandstone. An additional benefit of this rock type is that its microstructure is very similar to PFC3D particles.

A preliminary experiment that was performed involved loading a dry cylindrical sample of Crosland Hill sandstone in a standard uniaxial strength test. The results from this experiment were used to determine the basic material properties of the sandstone, that are essential for determining the PFC3D ‘Model of rock’ for this rock type.

Figure 14a is a photo of the polyaxial system. The system can perform tests on rock cubes of size 50.8 mm, and is one of only two in the World. The original six polyaxial platens contain sensors to measure p-, s1-, and s2-wave velocity. Since it was not feasible to incorporate AE sensors into these platens, a custom set of AE platens were designed and manufactured for the testing system. Four of these platens, each containing 4 AE sensors, are shown in Figure 14b. The polyaxial experiments were therefore divided into two:

- Experiment 1 - To determine static and dynamic moduli changes with load in the three principal directions.
- Experiment 2 - To record high-quality full waveform AE data on 16 receiving sensors, as well as regular 3D velocity surveys between 8 pulsing sensors and the receiving sensors.

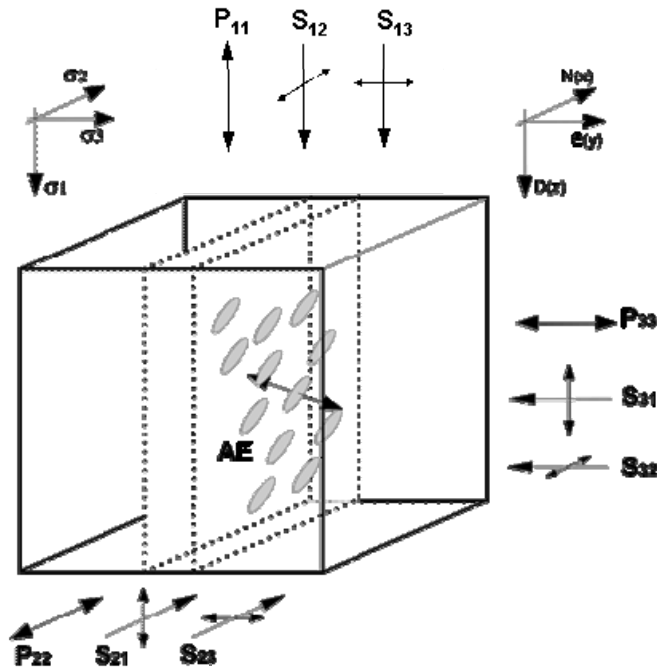


Figure 13: Summary of the ultrasonic monitoring capabilities during the polyaxial experiments. Definitions of the measured velocity components along the  $\sigma_2$  and  $\sigma_3$  directions are given e.g.  $P_{22}$  and  $P_{33}$ . The first numeral subscript refers to the direction of propagation and the second to the direction of particle motion.

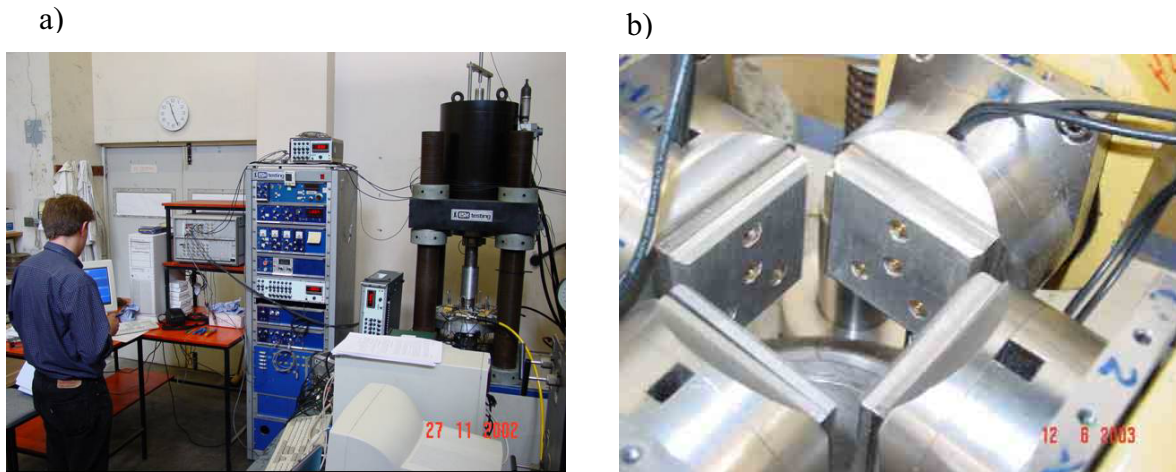


Figure 14: Photos of (a) the laboratory polyaxial system at Imperial College, London; and (b) details of the X and Y loading platens each containing 4 AE pinducer sensors.

The load history for Experiment 1 is presented in Figure 15. The initial part of the graph shows two hydrostatic loading cycles, where all three forces were increased and decreased equally. This allowed the effect of stress on a undamaged rock sample to be analyzed. The middle part of the graph shows a deviatoric cycle where the load in the x-axis was set at 5MPa, while the load in the y- and z-axis directions was increased to 100MPa. The z-axis was subsequently increased further, and then eventually the loads were reduced back to a low value. This cycle was chosen to induce an aligned microcrack set in the sample. The final two hydrostatic loading cycles were performed to look at the effect of stress on a damaged sample, in terms of rock modulus.

The staggered nature of the load history in Figure 15, is a result of a platen-based stress-probe measurement that was performed at 58 times during the test. The stress probe measurement essentially involved a small stress excursion, and was developed for SAFETI as a method to measure static moduli (elastic constant) values in each of the principal directions during the loading stages. To overcome time-dependent effects that were postulated to be occurring, Experiment 1

was repeated at a later time in the project, using a new rock sample and a slightly modified stress probe measurement in which a 30 second hold time was used during each probe excursion. This test is named Experiment 3. Unfortunately after processing the data from Experiment 3, it was still found that the method was not working as hoped, making the data incomparable with the modelled data, because strains were continuing to change after the 30 second period; thus, it was not possible to establish a well defined stress and strain change as required to compute the elastic constants. However, directly after each stress probe measurement, p-wave velocity, and the two polarised s-wave velocities were also measured in each of the principal directions. This velocity data can be interpreted in terms of dynamic elastic constants which can be directly compared to the modelled data.

The loading history for Experiment 2 is shown in Figure 16a. The first half of the stress-loading path is the same as Experiment 1, so that data can be directly related between the two experiments. However, the deviatoric cycle was continued until sample failure at 270 MPa, in contrast to Experiment 1 in which a maximum peak of 190 MPa was reached. The sample after the experiment contained visible macroscopic fractures, and future analysis is planned using thin section analysis. The axial strain in the three directions for Experiment 2 is shown in Figure 16b, and indicates opening in the y-direction, consistent with the visible fractures.

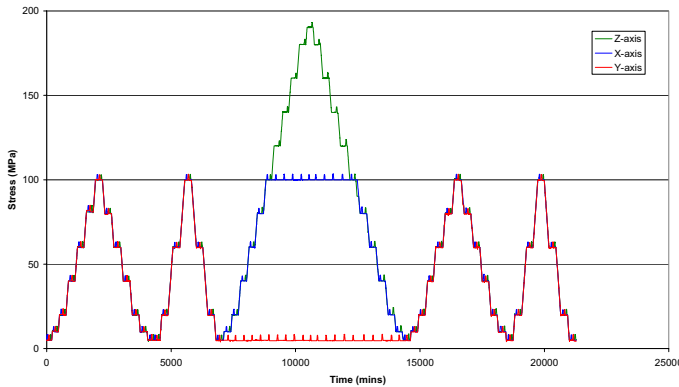


**Figure 15: The load history for Experiment 1, applied during the polyaxial test on Crosland Hill sandstone. The x-axis is time in minutes measured since the start of the test. The small stress-probe excursions can be seen.**

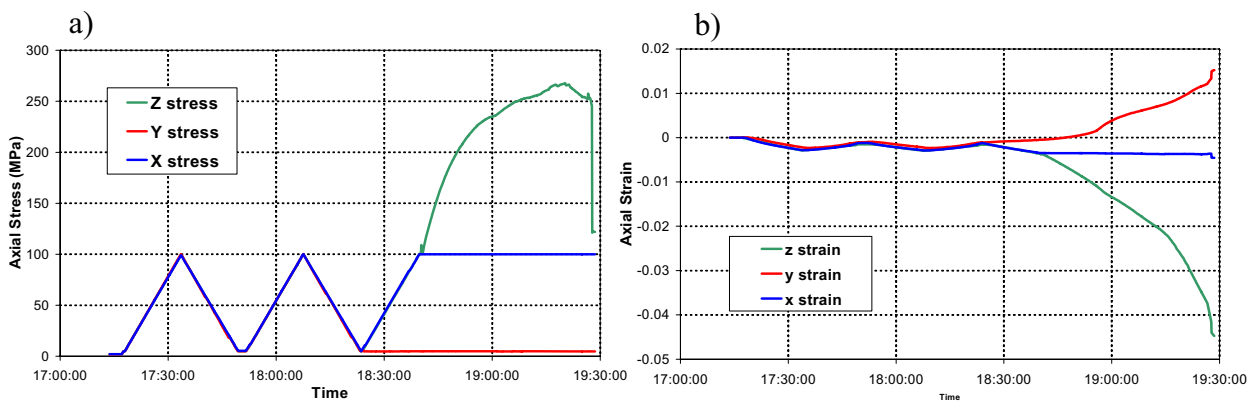


**Figure 16: a) The loading history for Experiment 2 applied to the three axes of the sample. b) Sample deformation recorded in the directions of the three axes.**

Figure 17 presents the calculated p- and s-wave velocities from Experiments 1 and 3. The velocities were calculated using a cross correlation technique with the uncertainty estimated to be  $\pm 25\text{m/s}$ . The velocities in the three directions show similar magnitude changes in the first two

hydrostatic loading cycles. In the deviatoric loading cycle, a significant reduction in the p-wave velocity in the y-direction occurs, suggesting that an aligned crack fabric has formed. It is noticed that a larger reduction occurs for Experiment 1, suggesting that this rock sample experienced more permanent damage, than the sample in Experiment 3.

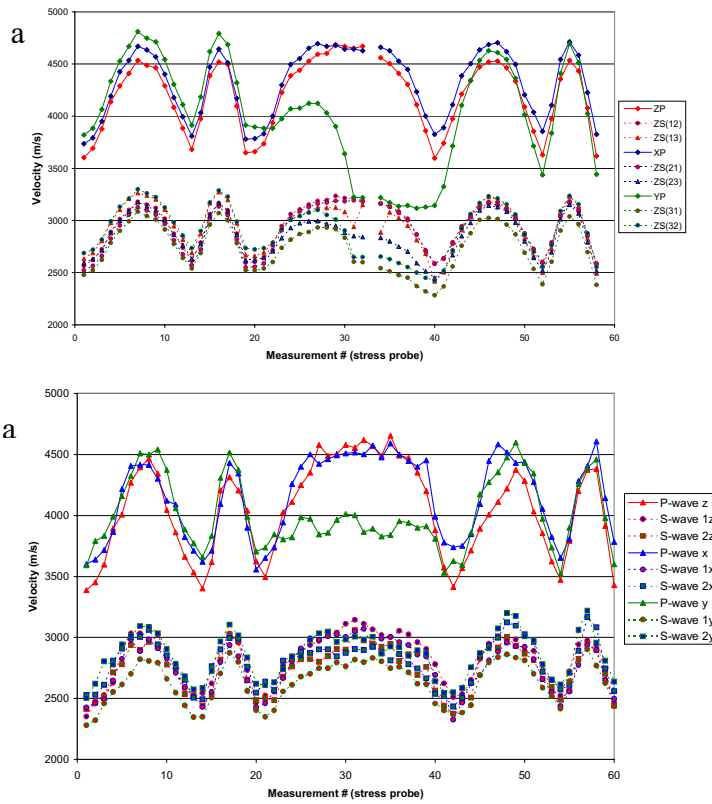


**Figure 17: P- and S-wave velocity values calculated for each of the three orthogonal directions through the cubic rock sample for (a) Experiment 1, and (b) Experiment 3.**

In Experiment 2, 38 ultrasonic velocity surveys were performed with time. Figure 18a presents an initial p-wave velocity stereonet of the rock sample, which shows the rock to be relatively isotropic. In Figure 18b, at the peak of one of the hydrostatic loading cycles, the velocity is still isotropic, but has increased by approximately 900 m/s in all directions. Figure 18c shows the velocity near the peak deviatoric stress, and there is a clear transverse anisotropy with the slow direction being W-E (y-direction), indicating an aligned fabric.

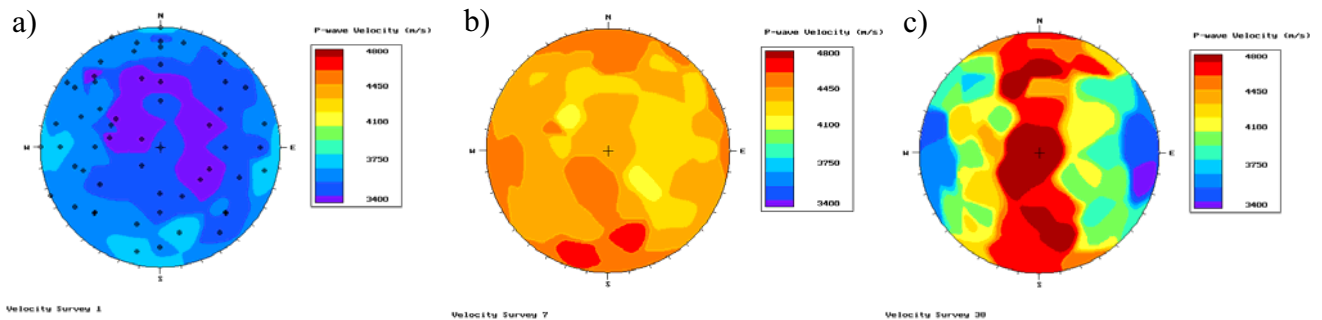


**Figure 18: P-wave velocity stereonet plots for Experiment 2, with (a) being the original unstressed rock; (b) after hydrostatical loading; and (c) after deviatoric loading.**

In Experiment 2, the AE ‘hit count’ data had 4 clear peaks suggesting the deviatoric ‘fracturing’ cycle may be composed of a number of fracture phases. All of the triggered AE waveform data was processed by picking arrival times and locating using a velocity model determined from the velocity survey data. Figure 19 presents the 9142 AE locations on three views of the rock sample. In the view looking in the x-direction (y-z plane), it is possible to interpret a number of macroscopic subvertical fractures.

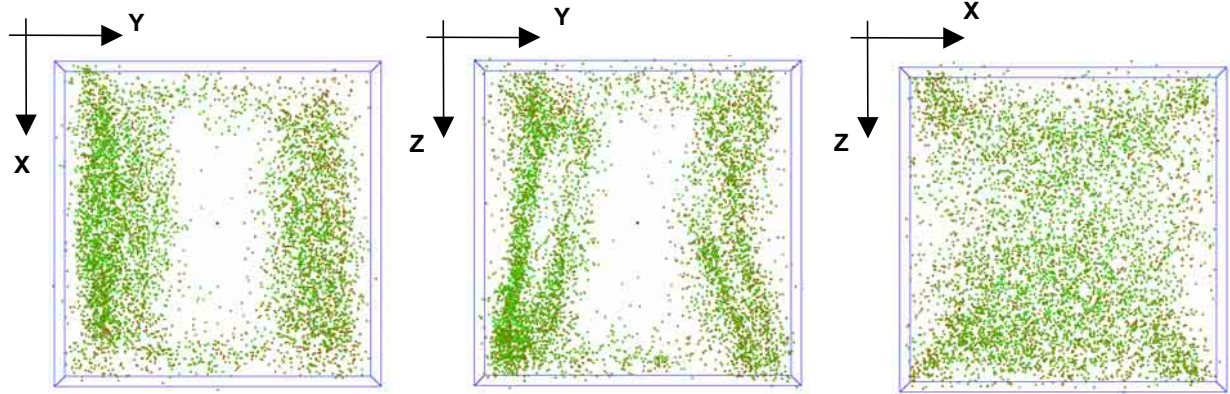


Figure 19: The AE locations for Experiment 2, shown on three orthogonal views of the cube.

## 2.6 EXCAVATION SCALE SEISMIC DATA SET

SKB’s Prototype Repository Tunnel (PRT) experiment was chosen as the excavation scale study for measured AE and ultrasonic velocity survey data. The PRT has been designed to simulate a disposal tunnel in a deep repository for storage of high-level nuclear waste. Its main objective is to test and demonstrate the integrated function of the repository components under realistic conditions on a full scale and to compare results with models and assumptions. The PRT consists of a 90m long, 5m diameter sub-horizontal tunnel excavated in Äspö diorite using a tunnel boring machine (TBM). Six full-scale deposition holes have been excavated vertically into the floor of the tunnel (Figure 20) using a TBM converted to vertical boring. Each measures 1.75m in diameter and approximately 8.8m in length.

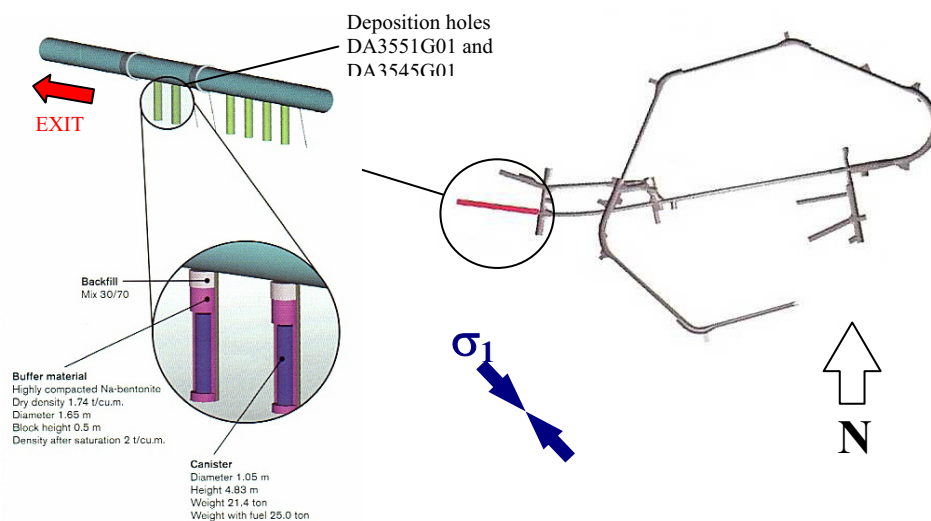
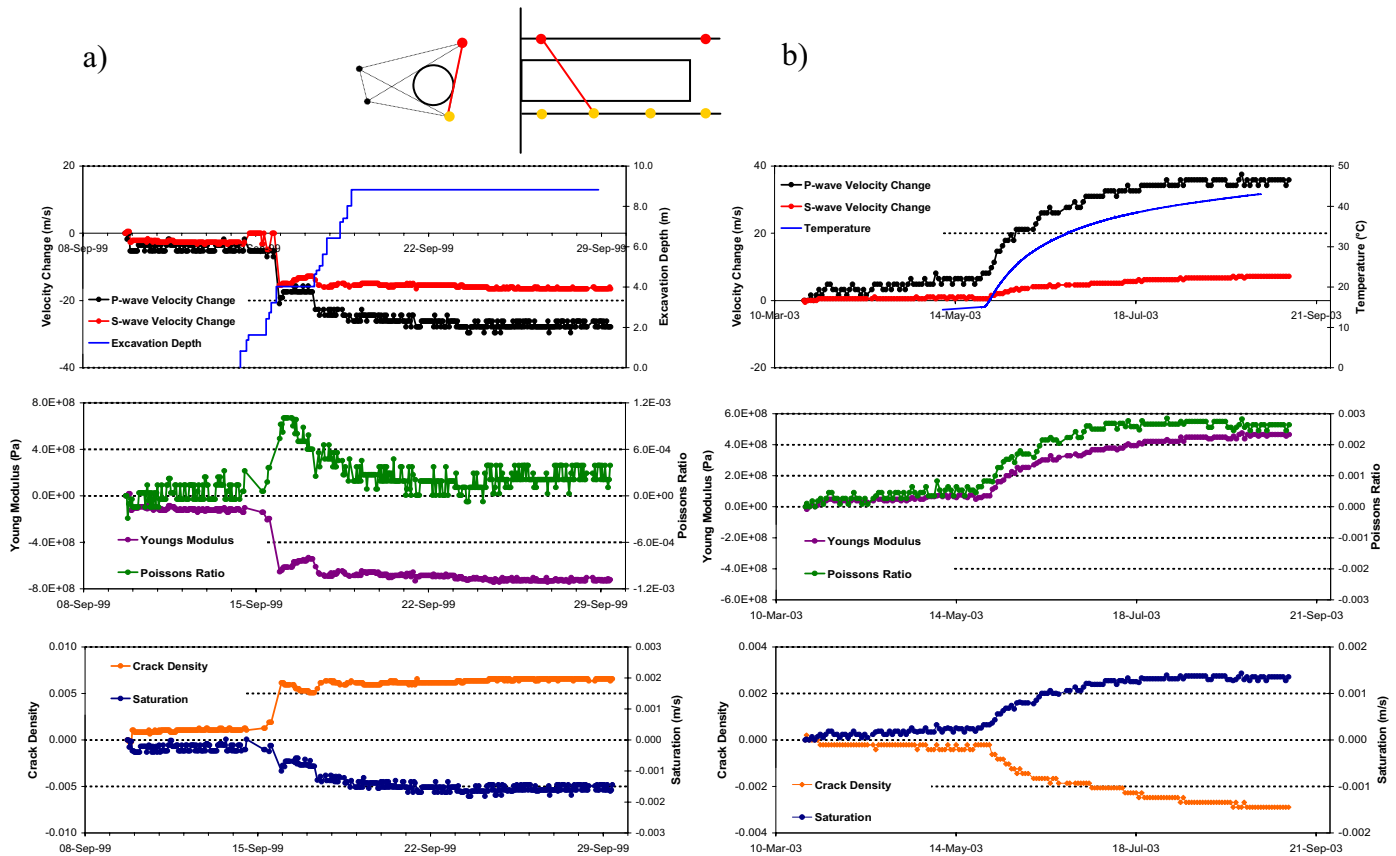


Figure 20: Plan view of the experimental tunnels at the Äspö HRL and the location of the Prototype repository. A schematic illustration of the final experimental set up is shown with canisters and bentonite clay installed in the 1.75m diameter deposition holes. Graphics are modified from SKB.



One of the deposition holes (DA3545G01) was monitored with an ultrasonic array during its excavation in 1999, and during a long term heating phase that started in 2003. The excavation consisted of eleven excavation ‘rounds’ of 0.8m, with a quiet monitoring period between each round. The sensors (transducers) were installed on ‘frames’ in small diameter vertical boreholes. The sensor array comprised of 8 transmitting sensors and 16 receiving sensors. An ESG Hyperion Ultrasonic System was used to monitor and collect the full waveform data. This system is the same type as the one referred to in the laboratory studies (Section 2.5). Both AE data and ultrasonic velocity survey data were recorded with time.

Velocity changes were measured between transmitter-receiver pairs using a cross-correlation technique. The greatest changes during the excavation were found to occur on raypaths skimming the deposition hole in the regions of high compressive stress. During the heating phase, a clear relationship of increasing velocity with temperature was observed. The increase is interpreted as closure of microcracks and pore spaces in the excavation damaged zone and surrounding rock. The velocity data was also interpreted in terms of changes in Young’s Modulus (E), Poissons Ratio, crack density (c), and saturation. Figure 21 presents the results for one of the raypaths that skims the deposition hole.



**Figure 21: The change in velocity, moduli, crack density, and saturation for raypath 1\_6 (transmitting sensor 1 to receiving sensor 6) during (a) the excavation phase; and (b) the heating phase of the PRT. This raypath skims the deposition hole as shown in the schematic.**

In total 884 AE events were located during the excavation phase (Figure 22a). The main distribution of events with azimuth around the deposition hole is approximately orthogonal to the maximum principal stress. 70% of the AEs locate within the first 20cm and 88% within the first 30cm. A few AE events locate about 1 meter from the deposition hole, and these are interpreted to be occurring on a pre-existing fracture. Although AEs locate down the full length of the deposition hole, they are not continuous down the length but instead locate in discrete clusters. It is possible these clusters occur on intersections between the deposition hole and pre-existing macroscopic

fractures. Figure 23 presents the time dependency of the events in relation to the excavation rounds. At the depth interval of any particular excavation round, in most cases, the majority of AE activity happens within the first 24 hours. However longer time dependency is also observed, with AE occurring up to 10 days after an excavation (10 days was the maximum monitoring time performed).

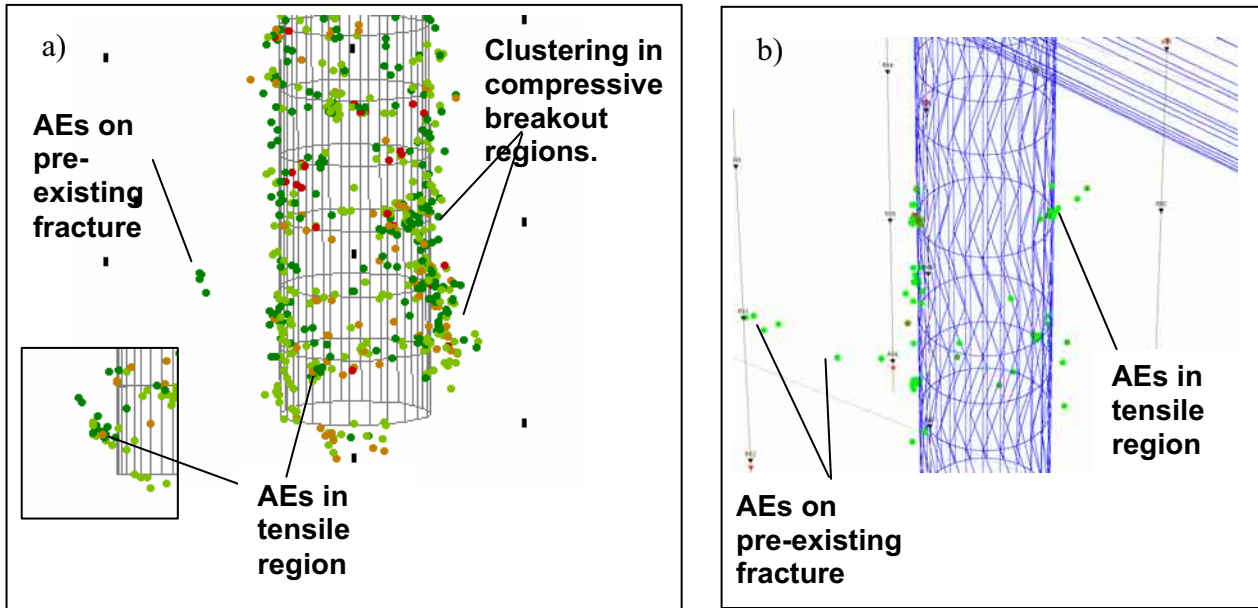


**Figure 22:** The majority of AE locations relative to the Prototype deposition hole during (a) excavation; and (b) heating.

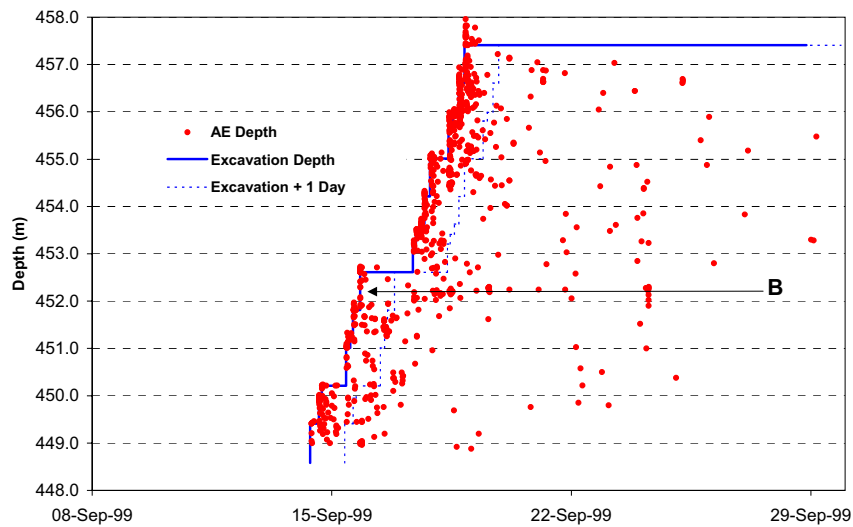


**Figure 23:** The time dependency of AE (red filled circles) at the difference excavation rounds. The solid blue line is the excavation depth and the dashed blue is the excavation depth displayed by 24 hours. Point B is an example of a cluster that develops over a period of about 8-9 days.

During the first four months of heating, 92 events were located (Figure 22b). Although the majority of the AEs locate within the first 20cm of the excavation perimeter, some disturbance in the rock mass further from the deposition hole is noticed. A total of 9 AEs were located at distance, and all occur at a similar height, suggesting a horizontal planar feature. The feature agrees with a set of semi-horizontal macroscopic fractures that are observed to intersect all the deposition holes in the PRT. Figure 24 presents the time dependence of the AE and the relationship with temperature.

A dramatic increase in activity around the end of June coincides with the temperature on the side wall reaching approximately 35°C.

Source mechanisms for a number of the events following the first 6 excavation rounds have been determined. Due to raypath coverage, the majority of successful solutions are for events occurring below the deposition hole.

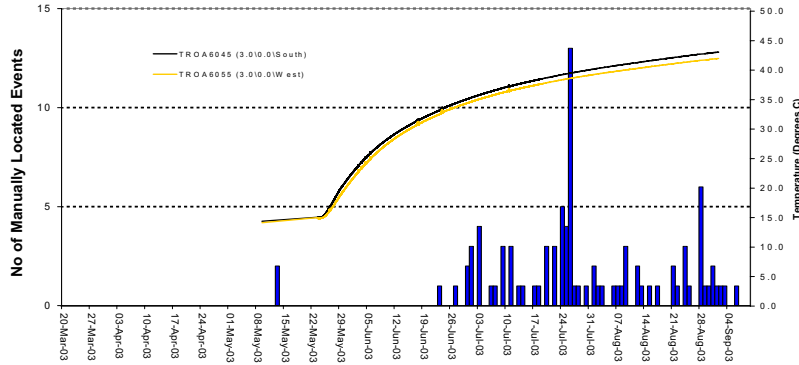


Figure 24: The temporal response of the AE with temperature change in the deposition hole.

## 2.7 MODELLING THE HYDRAULIC FRACTURE NETWORK

The simulation interpretation routines have been developed and tested, and a visualization method has been included for the created 3D-micro-fracture network and for the deduction of the corresponding hydraulic parameters.

The method involves first visualizing the created 3D-network, and then interpreting the fracture network in terms of hydraulic parameters. To get the corresponding hydraulic parameters, the 3D-fracture network data is written out and read into the groundwater code 3FLO. The hydraulic response can then be evaluated, based on simulations of uniform-gradient flow in the 3D-fracture network, parallel to the axis of the tunnel (Figure 25a). An equivalent permeability along the tunnel can be assessed by measuring the flow rates at boundaries (e.g. Figure 25b).

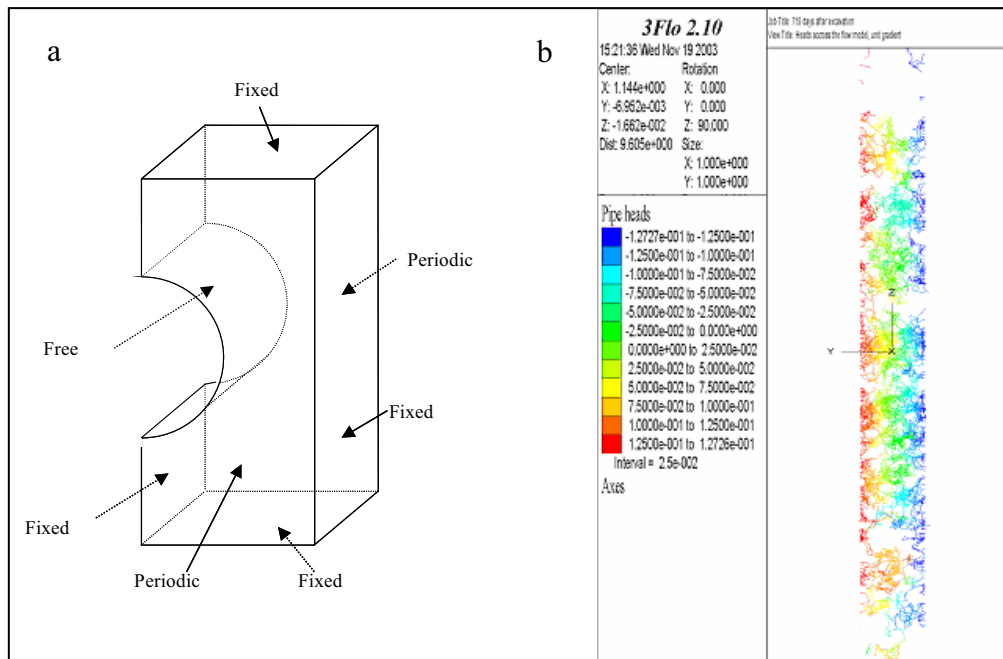


Figure 25: (a) Boundary conditions applied to perform the hydraulic tests (unit gradient), and (b) the pipe heads computed under a unit gradient, for a crack network existing 2 years after the excavation. Axis scale is 0.2m.



## 2.8 MODELLED RESULTS AND COMPARISON WITH MEASURED DATA

### 2.8.1 Laboratory

#### 2.8.1.1 Crosland Hill Sandstone Polyaxial Test

A PFC3D ‘model of rock’ for Crosland Hill sandstone was created and calibrated against measured strength test data. In order to have approximately 20 particles across each side of the cubic sample, an average particle diameter of 2.5mm was used. The stress-strain graphs for the measured and modelled data are similar, apart from the initial hardening response that occurs in the sandstone. The PFC3D material is already densely packed so that very little consolidation occurs. Modifying the PFC3D packing arrangement to obtain a more porous initial system was beyond the scope of this study but will be considered in future studies.

The model was subjected to the loading history displayed in Figure 15, but was only subjected to a maximum deviatoric stress of 115MPa, since it was found to fail soon after this value. A total of 51 stress probes and stiffness probes were performed throughout the modelled test using Methods SP and PS.

The PFC3D model was run ‘dynamically’ in order to simulate AE and velocity data. AE locations, magnitudes, and source mechanisms were calculated, as well as P- and S-wave velocity and stiffness values using Method WV.

Figure 26 presents a comparison of elastic stiffness values calculated from the two experiments and the three modelling methods. In all cases, the stiffness values in the principal directions (c11, c22, c33) increase during the hydrostatic loading and decrease during unloading. No permanent change in stiffness is observed in either case. It is encouraging that the model exhibits stiffness change with stress considering no constitutive relationships between stress and modulus have been specified. The stiffness changes are purely the result of compaction and formation of new contacts in the model. However the stiffness changes in the models (~5%) are much less dramatic than the measured values (~35%). It is likely that the large stiffness changes observed in the actual rock during hydrostatic loading are due to pre-existing cracks or pores that are closing under stress. Tests were performed on models with broken bonds prior to loading, but this did not significantly change the response. Future models will investigate methods for introducing pore space and/or inclusions of different materials.

The models exhibit a better quantitative match to the measured results (from Experiment 1<sup>1</sup>) during deviatoric loading when damage is induced. Both the model and actual rock show a significant decrease in stiffness in c33 (y-axis) of ~29% and ~37%, respectively. . The cause of the stiffness decrease in the models is the breaking of bonds and the opening of contacts due to redistributing forces. This is having a similar quantitative effect on modulus as the actual damage incurred in the sandstone through microcracking.

Figure 27 presents the modelled microcracks in 6 time periods during the peak failure period of the sandstone experiment. The microcracks in the first time period, form macrofractures oriented at about 35° from vertical, starting in the bottom left and top right corners of the cube. With time the initiation point of the macrofractures moves away from the corners, until in the last time step, the two interpreted macrofractures initiate almost vertically opposite each other. Also in the last time step, the orientation of the macrofractures are more subvertical, varying from about 15° to 30°.

In comparison, Figure 28 presents the measured AE locations divided into 6 time periods. Microfractures can be interpreted, and are seen to initiate near the corners and propagate across the sample. Initially fractures occur on the outer left and right of the sample, with a next phase of fracturing occurring more inwards in the sample. The last time period shows that a thin pillar of

---

<sup>1</sup> Note that in Experiment 3 less damage occurred than in Experiment 1, believed to be a result of slight differences in rock strength properties.

virtually intact rock still exists through the center of the sample, before failure. The interpreted macrofractures have orientations of  $5^\circ$  to  $25^\circ$ .

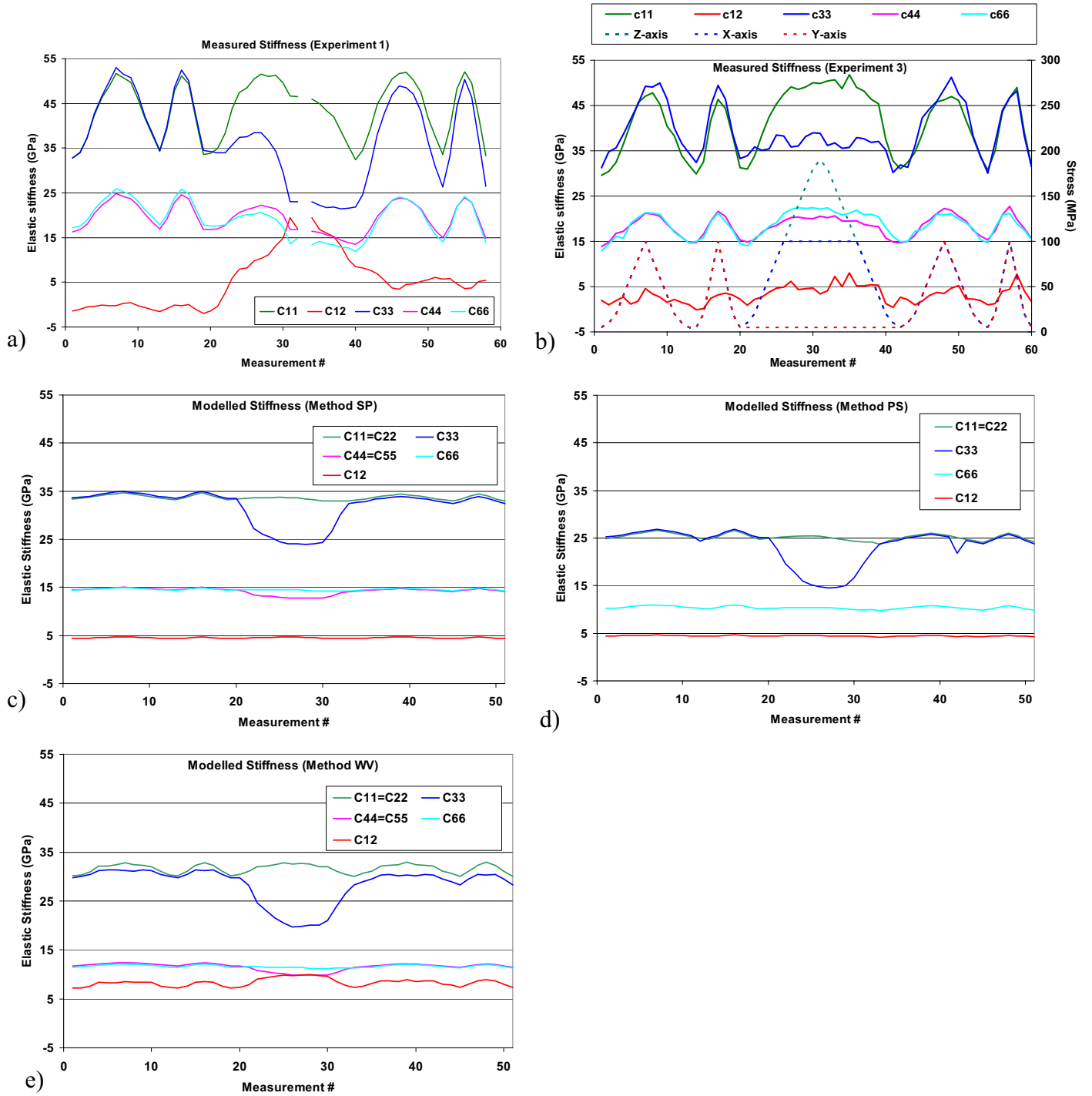


**Figure 26: Comparison of the measured (a,b) and modelled (c,d,e) elastic stiffness values from the polyaxial laboratory experiment.**

There are clear differences between Figure 27 and Figure 28, which may explain the lower failure strength for the modelled rock compared to the actual rock. However there are similarities as well, including where the macrofractures initiate from, their orientation, and the fact that there are multiple macrofractures. Source mechanisms of modelled AE from Figure 27 show the dominant pressure axis to be vertical (aligned with  $\sigma_1$ ) and the dominant tension axis to be

horizontal (aligned with  $\sigma_3$ ). This agrees with the forces acting during the deviatoric loading stage, and also is in agreement with the modelled stiffness values.

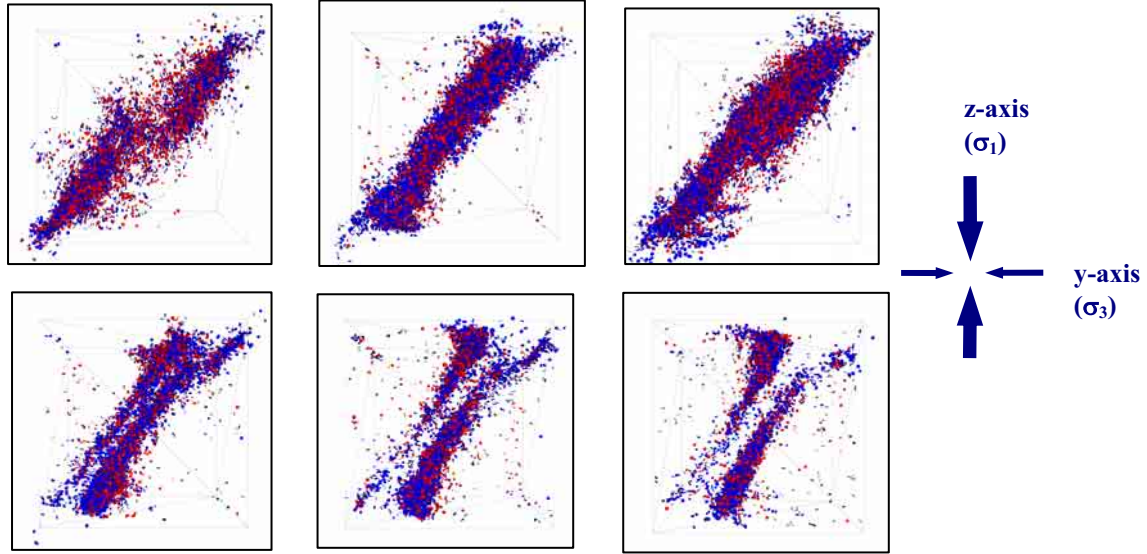


**Figure 27: The modelled microcracks during the peak failure stage of the polyaxial laboratory test on Crosland Hill sandstone, divided into six time periods.**

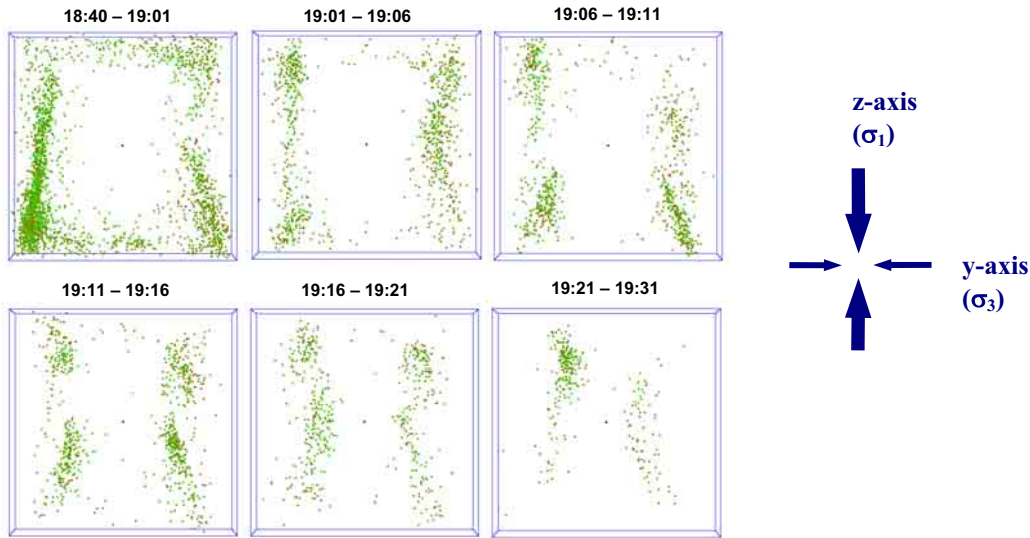


**Figure 28: The locations of the AE recorded during the polyaxial laboratory test, divided into six time periods.**

In order to investigate particle size issues, a higher resolution AC/DC model was produced of the sandstone experiment. The average grain size was reduced from 2.5mm to 0.55mm which is about double the 0.3mm actual grain size. In comparison to the first model with ~10K particles, this high resolution model had ~1 million particles. The model was created using 27 pbricks (each of ~40K particles), and run with AC/DC using 27 parallel processors. The model was subjected to one hydrostatic loading cycle followed by the deviatoric cycle. The model cube experienced a maximum stress of 180MPa without failure. When the cube was loaded past 180MPa, the programme crashed. Several attempts were made to rectify this but the problem persisted. The reason for the crashing is not known but it is likely due to the large volume of data being produced as millions of bonds are breaking during the macrofailure.

The million particle model did not run to complete failure but the strength was found to be greater than 180 MPa. This is significantly stronger than the coarser grained model which failed at ~130 MPa, and closer to the actual peak strength observed in the laboratory experiment (267MPa).

Similar strength increases with decreasing particle size for PFC3D materials are described by Potyondy and Cundall (2004). The reason for this size effect is unknown, although it is believed to correspond with general observations that finer-grained rock is stronger than coarser-grained rock. Although the particle size does affect the overall strength, it is suggested that changes to the representation of the modelled microstructure (adding in pre-existing open cracks and pore space) is likely to have more effect on the nature of failure, and these issues should be considered in the future.

### **2.8.1.2 SKB Äspö Diorite**

A ‘model of rock’ for Äspö diorite was determined. The microproperties of the modelled grains and cement were chosen to match compressive strength data and Brazilian tensile strength data measured from laboratory experiments on this rock type.

Unfortunately no long term strength data was available for the diorite. However a close analogue in terms of strength and composition is Lac du Bonnet granite. Synthetic static fatigue tests were performed with the diorite model rock, and the results were compared to long term strength data from the granite. This allowed the values of the long term model (Parallel bond stress corrosion model) parameters to be optimally determined.

### **2.8.1.3 Mont Terri Opalinus Clay Rock**

The strength and deformation test results from the Mont Terri site have been used to validate the constitutive model (failure criterion, crack initiation envelope and final failure envelope). Both short-term and long-term models have been calibrated by using experimental data from the Mont Terri site.

For the modelling and simulation of Opalinus clay it was essential to consider its layered structure, as it causes a pronounced anisotropic behaviour. In laboratory experiments this was taken into account by the preparation of three different types of axial-symmetric samples as shown in Figure 29.

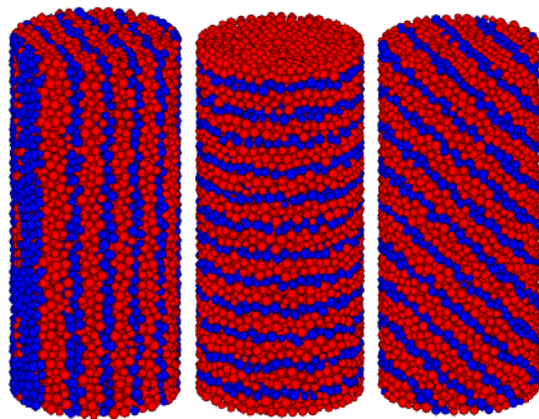


**Figure 29: P-, S-, and Z-sample used for modelling triaxial tests on Opalinus Clay at Mont Terri (blue = bedding planes, red = matrix material).**

When the samples were subjected to triaxial tests the confining pressure was always applied in the radial direction and the load was applied in the axial direction. Consequently, the axial load acts parallel (P-samples), perpendicular (S-samples) or inclined at 45° (Z samples), respectively, to the layered structure. Experimental investigations (Konietzky et al 2003) show that no scale effects

are evident. Hence, a calibration by means of these samples can be applied directly to the large scale model of the tunnel.

For the modelled samples, it is assumed that only the ratio between layer thicknesses is important, not the absolute amount. Thus, anisotropy was introduced by mesoscopic bedding planes and matrix planes. Different material properties were assigned to the sphere-bond systems according to their membership in bedding planes or matrix planes, respectively. Table 2 lists the geometrical parameters used in the modelled triaxial samples.

particle diameter	8 .. 12 mm
sample diameter	340 mm
sample height	770 mm
sample height / sample diameter	2.3
thickness of mesoscopic matrix plane	40 mm
thickness of mesoscopic bedding plane	20 mm
thickness of matrix plane / thickness of bedding plane	2
porosity at mean stress = 1kPa	0.36

**Table 2: Geometrical parameters of the numerical triaxial samples.**

For the calibration of the models, numerical uniaxial tests, triaxial tests and tensile tests on all three sample types were performed. The simulation results were compared to the parameters deducted from uniaxial laboratory tests, and the extrapolation of triaxial tests and anisotropy ratios from laboratory test samples from the Benken site location (Rummel et al 1998). These parameters are the result of an assessment of experimental results from different laboratories (Bock, 2001).

The most critical validation for the PFC model is the accurate reproduction of the fracture patterns observed in Opalinus clay. Figure 30 summarises and compares the observed and modelled fracture patterns. Z-samples show a clear macroscopic shear failure along the bedding planes. S-samples show a horizontal splitting along the bedding planes accompanied by shear band evolution. P-samples reveal vertical tensile splitting along the bedding planes coupled with shear band forming. Therefore, on p-samples and s-samples often a combination of tensile splitting along bedding planes and inclined shear fracture is observed. In contrast with this, z-samples exhibit pure shear fracture patterns along the bedding planes. All the observed fracture patterns are well reproduced by the model.

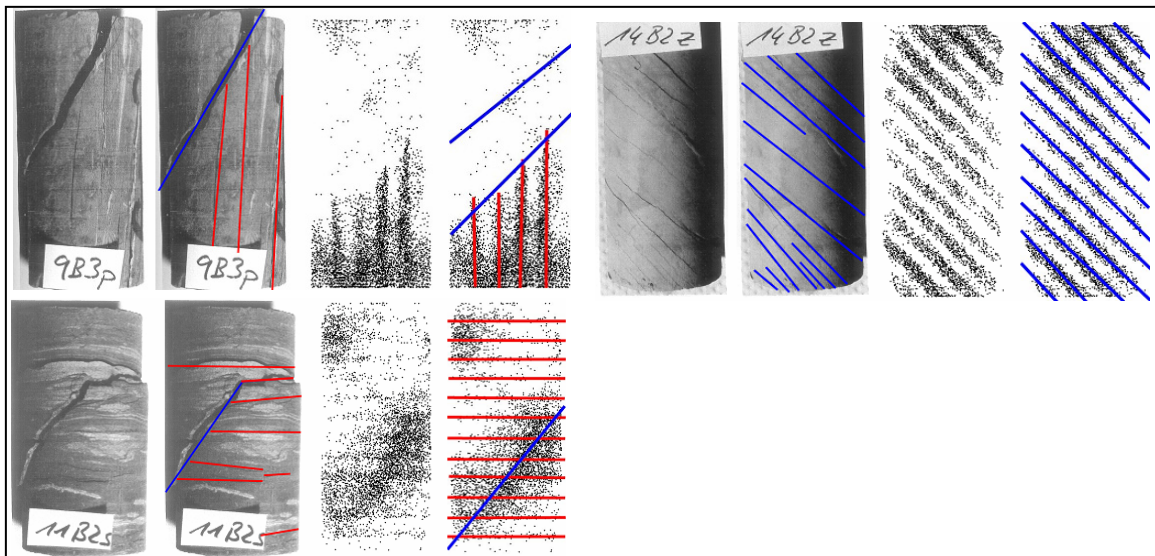


**Figure 30: A comparison of failure patterns for the 3 sample types. Blue is macroscopic shear failure, and red is macroscopic tensile failure.**



For the assessment of the long-term simulations only a few experiments were available from the Mont Terri site. A total of 9 data points for 3 specimens from Mont Terri as well as creep rates of Opalinus clay from the Benken site were used (Konietzky et al 2003). These data are widely scattered over a range of almost two decades. Therefore, only an order of magnitude can be estimated for the creep rates. The creep rates of the Mont Terri site are taken from creep tests over a period of 10 to 60 days. No creep test results are available for longer periods, so far. Therefore, in situ creep data were considered as well.

#### 2.8.1.4 Bure Callovo-Oxfordian Argillite

The short- and long-term macroproperties have been calibrated by performing triaxial tests and static-fatigue tests, respectively. In order to improve the results, some new phases have been introduced to build the initial sample. This includes: (1) generating particles and considering the stress state measured in-situ; (2) unloading the sample from the initial stress to almost zero; and (3) applying the PFC3D stress corrosion model in order to represent the time before the laboratory tests are performed, during which bond properties can change.

A number of laboratories have studied the short-term behaviour of this argillite (e.g. Chiarelli et al 1998; Gasc and Bauer 1998). Therefore a lot of experimental results were available to calibrate the numerical model. However, the difficulty was to choose which results should be used, since all these tests do not follow the same experimental process. It was chosen to consider the parameters fixed by ANDRA during the MODEX REP project (ANDRA 1999). Figure 31a shows the best calibration obtained by performing numerical triaxial tests at several confining pressures.

For the long-term parameters the problem was almost the same as for the short-term, since a lot of creep tests have been performed (e.g. G3S 2002; Zhang et al 2002). To calibrate the long-term parameters, several different creep tests were considered in order to validate the new model. Both single-step and multi-step creep test data were used. Additionally unconfined creep tests (Zhang et al 2002) as well as confined creep tests (G3S 2002) were considered. Figure 31b shows the best calibration obtained by performing a numerical multi-step confined creep test.

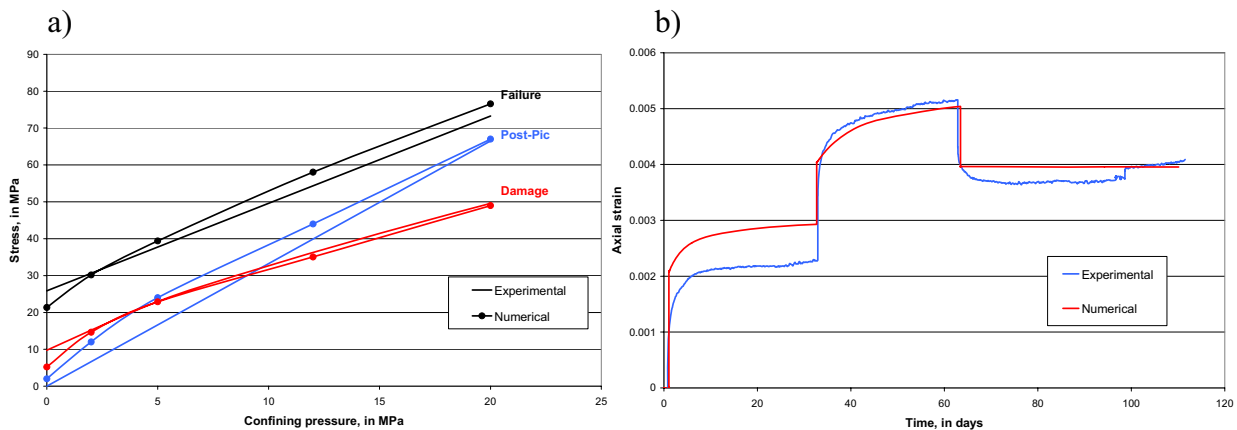


**Figure 31: A comparison of the experimental and numerical (a) criteria for the Callovo-Oxfordian argillite; and (b) multi-step confined creep test.**

## 2.8.2 Excavation Scale

### 2.8.2.1 SKB Diorite Prototype Repository Test

A large scale AC/DC model was produced of the SKB Prototype Repository Test (PRT). The main aim was to attempt to reproduce the acoustic emission (AE) pattern that was measured during the incremental excavation stages of the vertical deposition hole (Figure 22a).

The size of the final model was found to be limited by the RAM memory available on each processor (768Mb) of NESSC as well as a buffer size problem that appeared when too many processors were used to generate the model. Following a significant amount of testing, a final stable model configuration was decided. This used 640 pbricks, with each pbrick being 0.8m x 0.8m x 0.4m height, and containing 13700 particles. Each pbrick was assigned the 'model of rock' for diorite.

The model setup is shown in Figure 32, comprising a volume of 6.4m x 6.4m x 4.0m. The model allows two excavation increments of the deposition hole (radius 0.8m) to be performed. Modelled rock is present to at least 2.4m (3 radii) in all directions from the excavation. This distance was identified as the strict minimum required to avoid boundary artefacts, and to satisfy boundary stress conditions. The outer part of the model is composed of 280 degenerate matrix pbricks, the middle part of 200 matrix pbricks (with 2.7 million structural nodes), and the inner part with 160 particle pbricks (with 2.2 million particles). This represents the largest AC/DC model run on NESSC to date, and successfully used 40 processors operating in parallel.

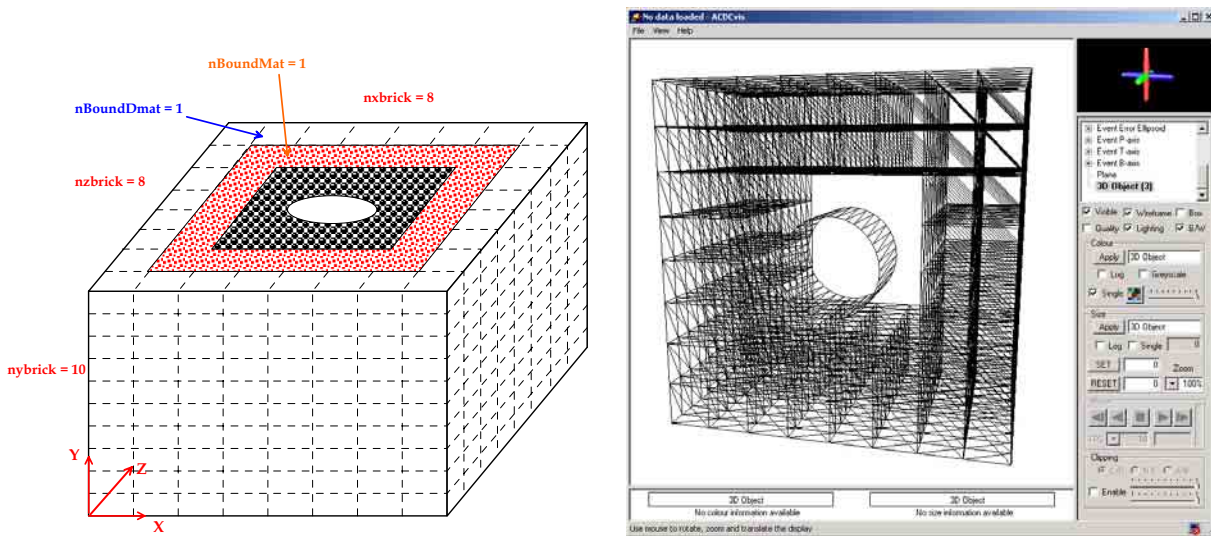


**Figure 32: Diagrams showing the setup of the AC/DC model of the SKB PRT. On the left, the black is particle pbricks, the pink is matrix pbricks, and the outer white grid is degenerate matrix pbricks. On the right, the pbricks and deposition hole are shown in ACDCVIS.**

Boundary stresses were applied to mimic the SKB PRT conditions. This involved applying a horizontal major stress ( $\sigma_1 = 30\text{MPa}$ ) along the x-axis, horizontal minor stress ( $\sigma_3 = 10\text{MPa}$ ) along the z-axis, and a vertical stress ( $\sigma_2 = 15\text{MPa}$ ) along the y-axis (deposition hole axis). These values were provided by SKB.

The first model runs using the calibrated bond strength of 208MPa showed that no microcracks occur around the deposition hole. This result was not unexpected. As discussed in Section 2.6, AE do not locate in a continuous band down the length of the deposition hole, but instead are interpreted to be occurring on intersections of the deposition hole with pre-existing fractures or zones of weakness in the rockmass that are under high stress conditions due to the excavation. Since it is beyond the scope of the project to add zones of weakness to the modelled

rock, a sensitivity study was performed to define the range of parallel bond strength that would allow crack generation in the model. The first microcracks around the deposition hole were obtained by using a mean bond strength of 43MPa. A value of 24MPa was interpreted to produce microcracks that were most realistic to the number and distribution of the measured AE.

A number of trials were made to use the stress corrosion algorithms with the large SKB model. However, for the first excavation step, it was found that convergence was not reached after 2 weeks of run time, and therefore due to time constraints, the long term algorithms were not used in the final modelling. Since a significant amount of the measured AE is recorded directly after an excavation increment, the model was still believed to produce relevant results for this project.

Figure 33 presents the modelled microcracks from two excavation steps on two side views.

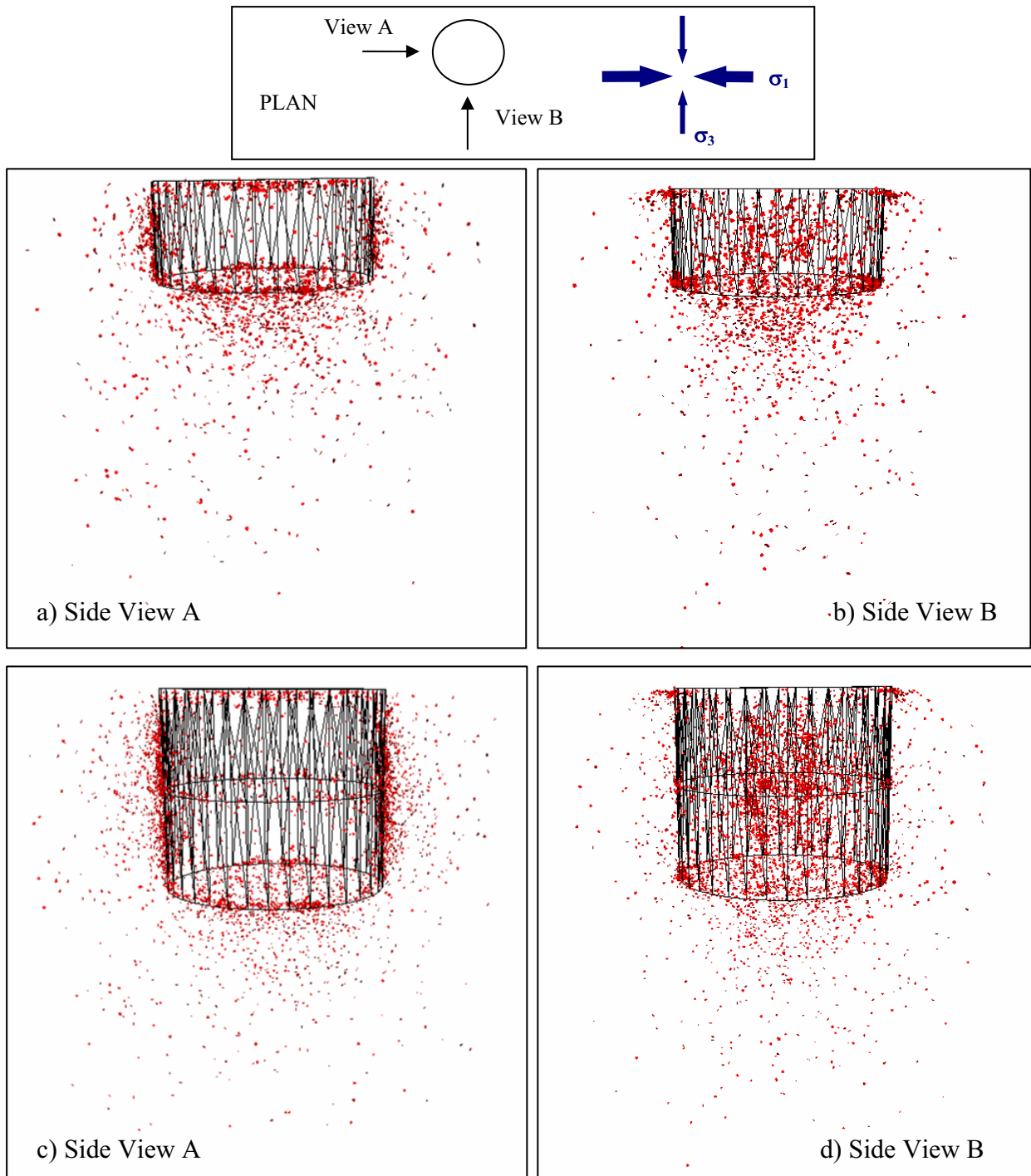


**Figure 33: All of the induced microcracks (bondbreaks) following two modelled excavation steps of the SKB PRT deposition hole. Mean bond strength is 24 MPa.**



The microcracks show clustering around the deposition hole in the  $\sigma_3$  direction, and also around the bottom of the excavation. It is noticed that the modelled microcracks extend significantly further into the rockmass than the measured AE. However it is also noticed that the microcracks occurring further out from the excavation occur at a later time than the ones near to the deposition hole, as a result of a time dependent stress redistribution.

Figure 34 shows a subset of the microcracks from Figure 33 occurring in a short time period directly after the excavation of the second excavation increment. Figure 35(ab) shows an enlargement of the plan view in Figure 34 focussing in on the deposition hole perimeter. For comparison, Figure 35c shows the measured AE. A number of similarities are seen between the modelled and measured data including significant clustering near the deposition hole perimeter in the  $\sigma_3$  direction, and less microcracking in the  $\sigma_1$  direction. Also significant modelled and measured microcracking is noticed to be occurring below the excavation. Source mechanisms of the measured AE below the excavation were found to be preferentially oriented sub-parallel (sub-horizontal) to the excavation. Figure 34 shows a significant portion of the modelled microcracks below the excavation to be sub-parallel.

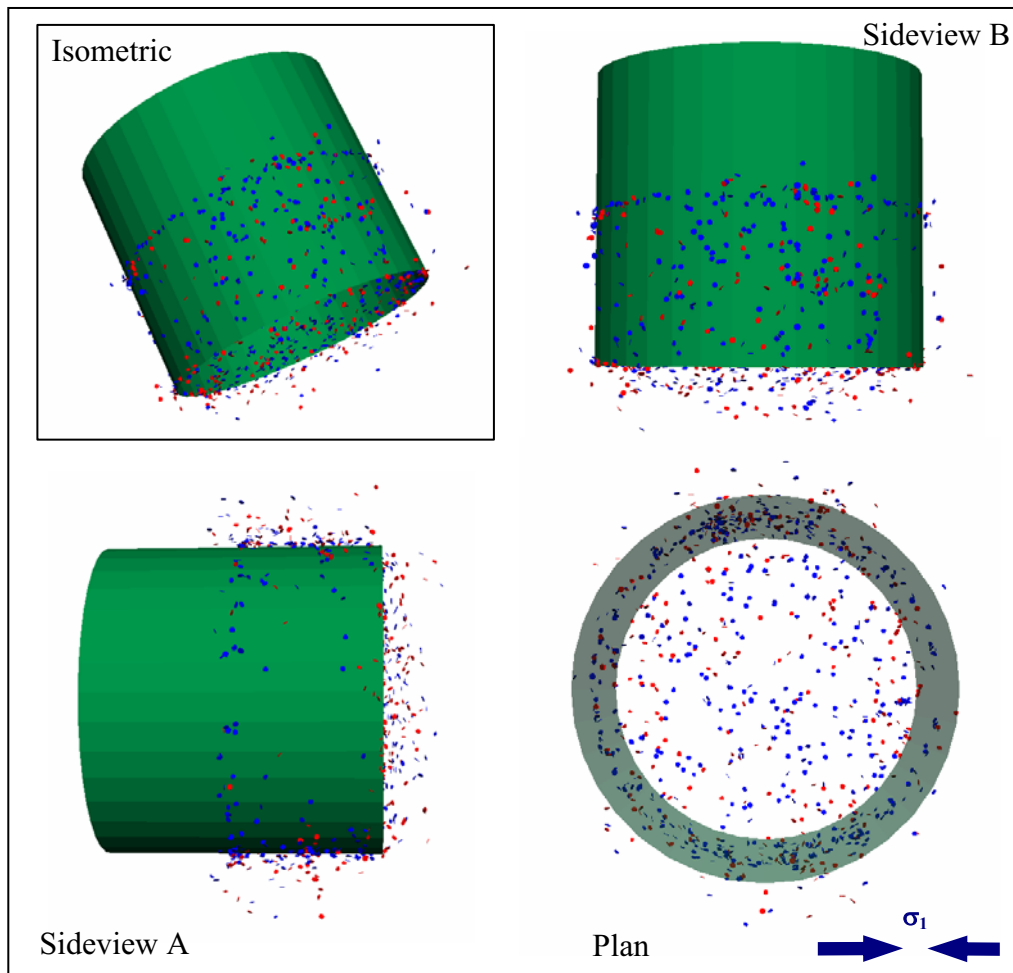


**Figure 34: The model of the SKB PRT, with 4 views (plan view is bottom right) showing the induced microcracks directly following the second excavation increment of the deposition hole. Tensile microcracks are shown in red, and shear microcracks in blue.**

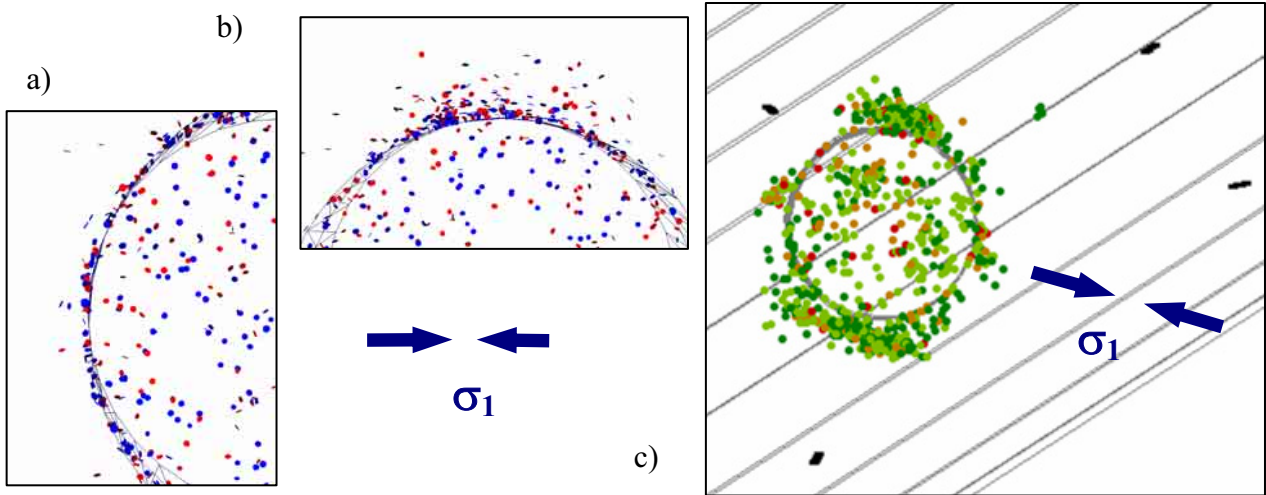


**Figure 35: A comparison of the modelled microcrack data (a,b) from Figure 34 and the measured AE data (c) for the PRT deposition hole. All views are in plan and relative to the indicated maximum principal stress orientation.**

### 2.8.2.2 Mont Terri Clay Excavation

Model runs simulating the Mont Terri experiment were performed with AC/DC. The following steps were followed to construct the numerical model: (a) construct a pbrick for Opalinus clay in periodic space, (b) apply the Mont Terri in-situ stress field into this AC/DC model, (c) use this pbrick to produce an AC/DC model of the region of rock surrounding the Mont Terri tunnel excavation, and (d) simulate the excavation by removing the particles in the tunnel region, and subsequently monitor the deformation and damage.

The initial numerical model (only one half of the cylindrical excavation was modelled) is composed of 17 pbricks in the horizontal direction (4.4 m width) and 34 pbricks in the vertical direction (8.8 m height). Along the tunnel axis, one pbrick was used (0.26 m depth), and a periodic boundary condition was applied. Thus, the model was composed of 578 pbricks, corresponding to 1.6 million particles. In order to carry out this study, AC/DC was run on four 3.0 GHz parallel processors, each having a minimum of 1Gb of RAM. The model was divided into four horizontal planes, containing respectively 9, 8, 8, and 9 zones. Five rows of matrix pbricks were used along the three boundaries that did not contain the tunnel. Thus, 280 matrix pbricks were initialised, which had the effect of doubling the speed of the numerical simulation and gaining about 25% of RAM usage. A criterion was defined for automatically adaptively switching matrix pbricks into particle pbricks, when the number of cracks equalled 1% of the initial number of parallel bonds. When the criterion was reached in a particle pbrick, all the matrix pbricks around this particle pbrick are converted.

The excavation phase was simulated by removing particles in the tunnel region. The forces previously applied by the removed particles were first added at the tunnel boundary, and then slowly reduced, in order to mimic the excavation procedure, and avoid crack artefacts around the tunnel. When a steady-state stress was reached, the long term model was run for a period of 2 years.

During the first two years, the model indicates crack propagation up to 25 cm from the tunnel perimeter (Figure 36). The number of connected cracks increases rapidly during the first 6 months, then remains virtually constant after one year. A statistical analysis of the connected microcracks versus depth and angle is shown in Figure 37. The evolution of the displacement field was also studied (Figure 38).

The model has been interpreted in terms of the fracture network and equivalent permeability by using the developed 3FLO software. This allows the micro-fracture distribution to be interpreted in terms of:

- hydraulic parameters of the EDZ (permeability, porosity)
- pore water pressure distribution
- expected water inflow into the drift

All of these results have been recorded as a function of time.

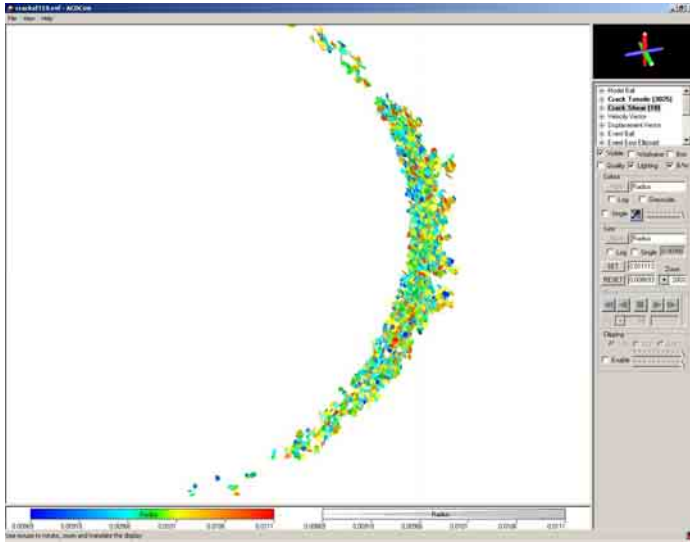


**Figure 36: Micro-cracks connected after two years of the shaft excavation at Mont Terri.**

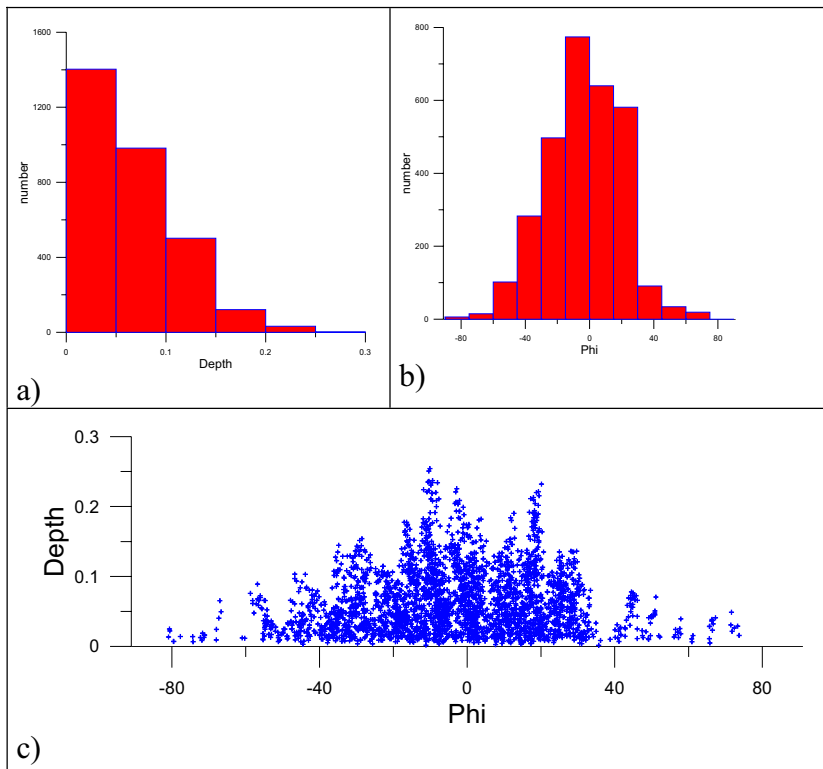


**Figure 37: The microcracks around the shaft excavation after two years, with (a) presenting the number of microcracks versus depth in meters, (b) the number of microcracks versus angle in degrees, and (c) depth versus angle.**

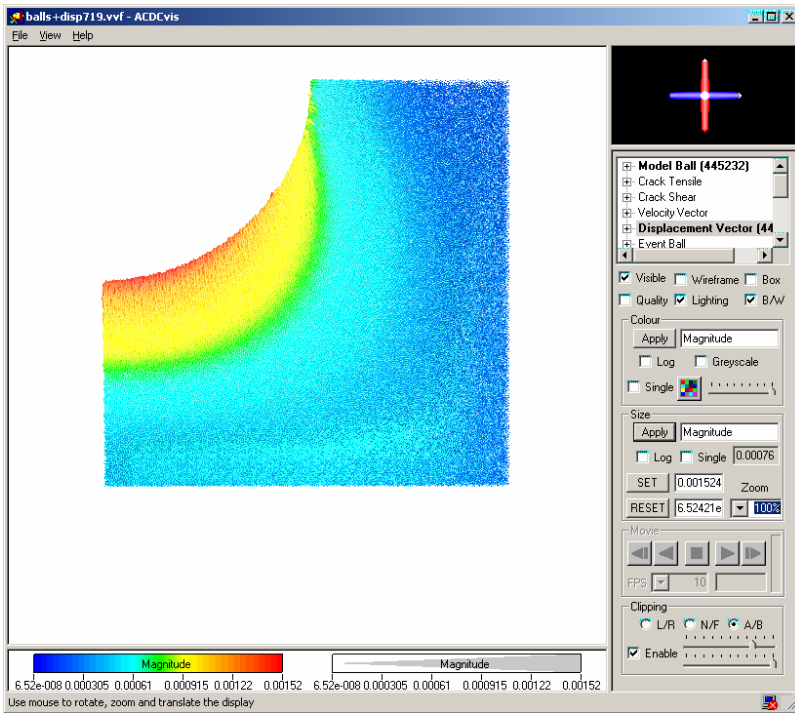


**Figure 38: The displacement field around the Mont Terri excavation after two years.**

### 2.8.2.3 Bure Argillite Prediction

Similar to the modelling in Section 2.8.2.2, the model excavation inside the Callovo-Oxfordian argillite was performed on four 3.0 GHz parallel processors, each of them having 1 or 2 Gb RAM, and connected by a 1 Gb/s network .

As the Bure argillite is only weakly anisotropic, it is assumed to be isotropic in the model. Therefore only a quarter of the excavation was required to be modelled. The procedures used were similar to the Mont Terri study. Three numerical models were run in order to study several excavation orientations (vertical or horizontal), depths (from 465 to 500 m), and the building of a liner (after 50 or 180 days of the excavation opening). These three models contain from 0.4 - 1.4 million particles.

The procedure for the definition of the hydraulic properties of the equivalent microcracks network was improved. A square law defining the variations of transmissivity with fracture thickness was obtained and calibrated (Figure 39), by using a set of experimental tests run by the Ecole Centrale de Lille (Skoczylas 2004). This law was then used to calculate the variations of permeability around the excavation versus time.

The results of the simulations are plotted using several representations: (1) view of the connected microcracks (Figure 40); (2) representation of number of microcracks versus the depth (i.e. distance from the tunnel wall) and angle; (3) evolution of the permeability versus time (Figure 41a); and (4) analysis of the effect of the liner (Figure 41b).

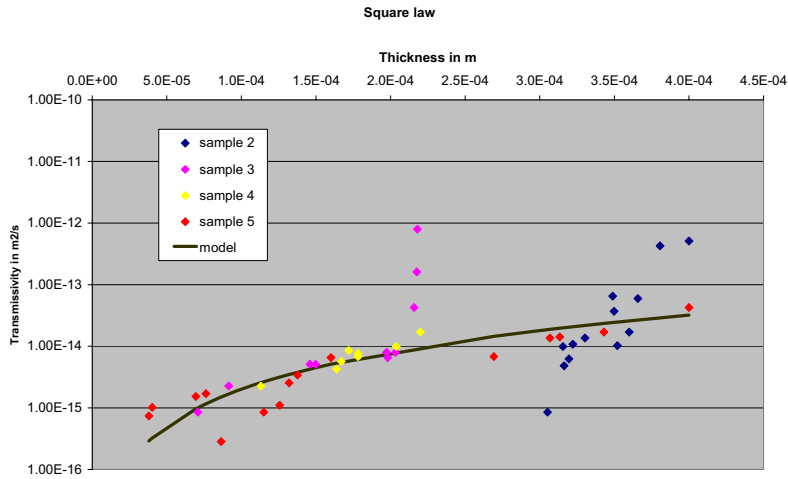


**Figure 39: Representation by a ‘square law’ of the transmissivity versus fracture thickness for the Bures argillite.**

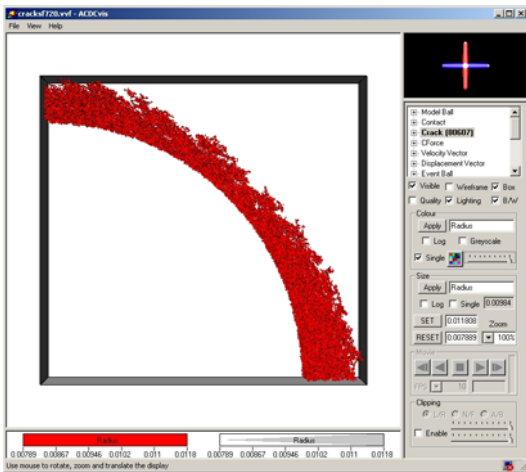


**Figure 40: The connected microcracks after 720 days for an excavation in the Bures argillite.**

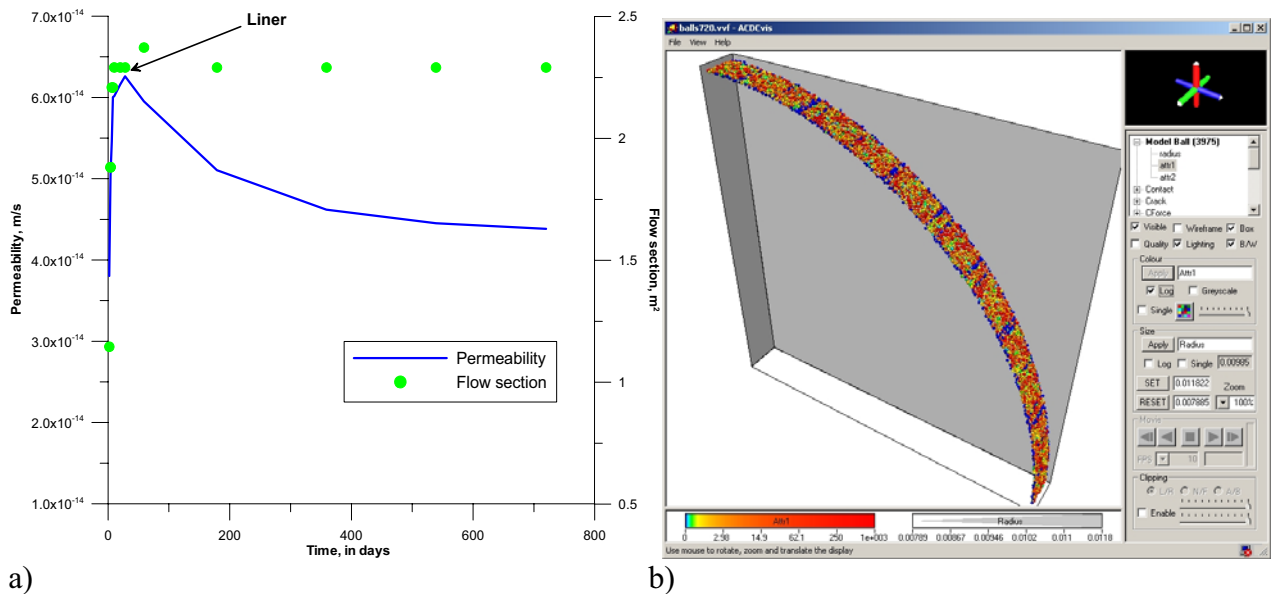


**Figure 41: The(a) variation of permeability and flow area around the excavation during the first two years; and (b) visualisation of the forces (in log notation) on the liner after 720 days.**

### 3 ASSESSMENT OF RESULTS AND CONCLUSIONS

The major objective of SAFETI, to develop and validate a new innovative 3D numerical modelling procedure, has been achieved.

The main conclusions are:

- The 3D modelling code AC/DC (Adaptive Continuum/DisContinuum) has been developed and implemented. The code runs on Linux and was successfully tested and used on 40 processors of the parallel supercomputer cluster (NESSC) at Liverpool University, England. Additionally it was successfully used on a fast 4 parallel computer cluster in France.
- The visualization software (called ACDCvis) has been developed and tested. The software allows users to remotely analyze the AC/DC model and compare with measured data. The software runs under Windows and contains a suite of 3D spatial and temporal visualization and analysis techniques, making use of graphics card technology.
- Procedures have been developed for accurately and efficiently producing PFC3D and AC/DC 'Models of Rock'. This includes isotropic rock types as well as rock types with layered (bedding) structures at various orientations.
- Algorithms have been developed for analyzing PFC3D and AC/DC 'Models of Rock', including static and dynamic elastic modulus and AE/MS (acoustic emission/microseismic) activity in 3D.
- Algorithms have been developed for PFC3D and AC/DC that mimic the long-term damage processes in rock. This includes a stress corrosion law suitable for granite and diorite, as well as a creep law appropriate for argillite and clay rocks.
- A method has been produced for interpreting and visualizing the hydraulic fracture network in an AC/DC model, and calculating the corresponding hydraulic parameters.
- A validation dataset has been produced from a polyaxial laboratory loading test on Crosland Hill sandstone at Imperial College London. A loading history was used which induced a microcrack structure into the rock sample, and also allowed the effect of stress on undamaged and damaged rock to be investigated. The dataset includes interpreted full waveform AE and modulus data with time throughout the experiment.
- A PFC3D and AC/DC model of the polyaxial laboratory test shows a number of similarities to the measured data.
- A calibration dataset has been produced from a field scale excavation at SKB's hard rock laboratory in Sweden at 440m depth. The dataset includes AE and modulus data with time throughout the incremental excavation phase of the deposition hole, as well as the subsequent heating phase of the experiment.
- An AC/DC model of the SKB field scale deposition hole excavation has been produced that shows a number of similarities to the measured AE data. The model has 160 particle pbricks (with 2.2 million particles), 200 matrix pbricks (with 2.7 million structural nodes), and 280 degenerate matrix pbricks, and represents the largest AC/DC model successfully produced to date.
- AC/DC models of field-scale excavations of the Callovo-Oxfordian argillite at Bure France, and of the Opalinus clay at Mont Terri Switzerland have also been performed. The fracture networks over a 2 year period were modelled, and the corresponding hydraulic parameters were determined.

AC/DC represents a major advance in the size of 3D discrete element (particle) models that can be simulated. The SAFETI project uses novel procedures and parallel computing power to produce models of 3D field-scale experiments, that overcome previous computer limitations of discrete element modelling. AC/DC is a code that can be used in any brittle materials such as rock

or concrete, and allows the user to model volumes subjected to insitu 3D stress fields and excavation geometries. It allows the resulting spatial and temporal microcrack behaviour and modulus change to be analyzed, and provides the user with a powerful tool to determine optimal geometries, and geomechanical parameter sensitivities. The main input values required for the model are insitu stress measurements and parameters determined from standard rock tests including Young's modulus, Poisson's ratio, crack-initiation stress and uniaxial compressive strength (UCS).

The primary aim of AC/DC is as a tool for nuclear repository development programs. At the early stages of site selection and characterization, the code provides a method for predicting the microcrack response of different rocktypes to excavation and stress. For repository layout design, AC/DC provides a method for analyzing the excavation damage zone (EDZ) development from different deposition hole spacing. It also provides an essential method for estimating the long term response and stability of the facility over time periods of thousands of years.

The AC/DC code is being marketed by the industry partner Itasca to current users of PFC3D as well as other companies, universities, and research institutes in the fields of nuclear waste management, civil engineering, petroleum, and earth sciences. The industry partner ASC is marketing the use of seismic monitoring methods for AC/DC model validation. A significant amount of the marketing of the codes and methods is being performed by all project partners through journal and conference publications. AC/DC will benefit from the guaranteed future improvements in computing power, that will allow ever larger and higher resolution models to be created.

## 4 ACKNOWLEDGEMENTS

The partners gratefully acknowledge the partial funding of this project by the European Commission as part of the fifth EURATOM framework programme, Nuclear Fission (1998-2002). SKB and ANDRA are thanked for their involvement in the project as unfunded partners.

## 5 REFERENCES

- ANDRA (1999). Geological Statement Report on the Eastern Site, Rapport ANDRA #ARPADS99-005/1.
- Bock, H. (2001). RA Experiment - Rock Mechanics Analyses and Synthesis: Data Report on Rock Mechanics, Technical Report TR 2000-02 by Q+S Consult, Mont Terri Underground Rock Laboratory.
- Chiarelli, A., S., Kondo, D., and Shao, J. F. (1998). Rapport de Synthese sur les argilites de l'Est, Rapport ANDRA #BRP0LML98-001/A.
- Gasc, M., and Bauer, C. (1998). Comportment Differe Compte Tenu des Couplages Thermo-Hyro-Mecaniques des Argilites Silto-carbonatees de l'Est, Rapport ANDRA #BRP0G3S98-007/A.
- G3S (2002). Rapport ANDRA #DRPG3S02-004/A.
- Hanks, T. C. and H. Kanamori (1979). A moment magnitude scale, *Journal of Geophysical Research*, 84: 2348-2350.
- Hazzard, J. F., and Young, R. P. (2000). Simulating Acoustic Emissions in Bonded-Particle Models of Rock, *International Journal of Rock Mechanics*, 37 (5), 867-872.
- Jaeger, J. C. and N. G. W. Cook (1969). Fundamentals of rock mechanics, London, Methuen & Co., Ltd.
- Konietzky, H., Blumling, P., teKamp, L. (2003). Opalinuston – Felsmechanische Untersuchungen, Interner Bericht 03-08, ITASCA Deutschland & NAGRA Schweiz.
- Kranz, R.L., and Estey, L.H. (1996), Listening to a Mine Relax for Over a Year at 10 to 1000 Meter Scale, *In Proceedings of the 2<sup>nd</sup> North American Rock Mechanics Symposium*, Balkema, 491-498.
- Kuhlemeyer, R. L. and Lysmer L. (1973). Finite Element Method Accuracy for wave Propagation Problems, *Journal of Soil Mechanics and Foundations*, 99, 421-427.
- Lei, X., K. Kusunose, et al. (2000). Quasi-static fault growth and cracking in homogeneous brittle rock under triaxial compression using acoustic emission monitoring, *Journal of Geophysical Research* 105: 6127-6139.
- Madariaga, R. (1976). Dynamics of an expanding circular fault, *Bulletin of the Seismological Society of America* 66: 639-666.
- Moore, D. E. and D. A. Lockner (1995). The Role of Microcracking in Shear-Fracture Propagation in Granite, *Journal of Structural Geology* 17(1): 95-114.
- Potyondy, D. O., P. A. Cundall and C. Lee (1996). Modelling Rock Using Bonded Assemblies of Circular Particles. *Proceedings of Second North American Rock Mechanics Symposium NARMS'96*, Montreal, Canada, A.A.Balkema.
- Potyondy, D. O. and P. A. Cundall (1998). Modelling Notch-Formation Mechanisms in the URL Mine-by Test Tunnel using Bonded Assemblies of Circular Particles. *Proceedings of Third North American Rock Mechanics Symposium NARMS'98*, Cancun, Mexico.
- Potyondy, D. O. and P. A. Cundall (1999). Modelling of Notch-Formation Mechanisms in the URL Mine-by Tunnel: Phase IV: Enhancements to the PFC Model of Rock, Ontario Hydro Nuclear Waste Management Division Report, 06819-REP-01200-10002-R00.
- Potyondy, D. O. and P. A. Cundall (2001). The PFC Model for Rock: Predicting Rock-Mass Damage at the Underground Research Laboratory, Itasca Consulting Group Inc., Report to Ontario Power Generation #06819-REP-01200-10061-R00.
- Rummel, F. et al. (1998). Laboratory Experiments for the Determination of Deformation Mechanisms and a Constitutive Law for Time-dependent Deformation Behaviour of the Opalinus Clay, Technical Note TN 98-55.
- Scholz, C. (1990). The mechanics of earthquakes and faulting. Cambridge, Cambridge University Press.
- Skoczylas, F. (2004). Project HAVL, Rapport provisoire: Mesure de Permeabilities au gaz et a l'eau sur l'argile fracturee, Rapport ANDRA #CRP0ECL04-002/1.
- Tapponnier, P. and W. F. Brace (1976). Development of stress-induced microcracks in Westerly granite, *International Journal of Rock Mechanics and Mining Sciences & Geomechanics Abstracts* 13: 103-112.
- Young, R. P., Collins, D. S., Reyes-Montes, J. M. and Baker, C. (2004). Quantification and Interpretation of Seismicity, *International Journal of Rock Mechanics*, 41, 8, 1317-1328.
- Zhang, C, Dittrich, JI, Muller, J., and Rothfuchs, T. (2002). Experimental Study of the Hydromechanical Behaviour of the Callovo-Oxfordian Argillites, GRS, June.



## 6 GLOSSARY

$\sigma_1$	Maximum stress vector (direction and magnitude)
$\sigma_2$	Intermediate stress vector (direction and magnitude)
$\sigma_3$	Minimum stress vector (direction and magnitude)
AC/DC	Adaptive Continuum/DisContinuum code
ACDCvis	Software for 3D visualisation and analysis of results produced by AC/DC or PFC3D models and laboratory or insitu seismic data sets.
AE (Acoustic Emission)	Small, high frequency seismic events – recorded by seismic sensors in the frequency range ~30-500kHz, with moment magnitude on the order of $-7$ to $-5$ .
AECL	Atomic Energy of Canada, Ltd.
Attenuation	The loss of energy as a wave travels through some dissipative medium
Bond	Connects PFC particles to provide strength to simulated rocks
Continuum model	Material is assumed to be continuous with few faults, joints or spaces
Crack	Single bond breakage in PFC model
Damping	Extraction of energy from model to simulate attenuation
Discontinuum model	Material is assumed to be composed of independent elements free to move relative to each other
FISH	Programming language for PFC and AC/DC. Files are named ‘*.FIS’.
HRL	Hard Rock Laboratory, part of Aspö’s facilities for the study of nuclear waste disposal in Sweden.
INSITE	Seismic processing software produced by ASC Ltd.
Magnitude	(also moment magnitude). A logarithmic measure of earthquake strength
Microcrack	See <i>crack</i>
Microproperty	Properties assigned to particles and bonds in PFC
MS (Microseismic)	Seismic events larger and lower frequency than AE but smaller than traditional earthquakes. With a frequency range of approximately 0.5 – 20 kHz, and moment magnitude of the order $-4$ to $-2$ .
Modulus	Stiffness (see Young’s Modulus)
Moment tensor	A mathematical description of the mechanics of a seismic source
MPI	Message Passing Interface – language used in parallel processing.
NESSC	Networked Earth Science Supercomputing Cluster at Department of Earth Sciences, Liverpool University
Particle	A single spherical element in PFC
PFC	Particle Flow Code produced by Itasca.
Poisson’s ratio	An elastic constant defined as the ratio of transverse strain to longitudinal strain.
Q (Quality factor)	A measure of the seismic quality of a material. Inversely proportional to attenuation.
URL	Underground Research Laboratory, part of Atomic Energy of Canada’s facilities for the study of nuclear waste disposal.
VVF	Versatile file format imported into ACDCvis
Young’s Modulus	An elastic constant defined as the stress-strain ratio when a rod is pulled or compressed.

## 7 APPENDIX 1 — LIST OF DELIVERABLES

The itemised list of deliverables is presented in Table 3.

Item	Report of Deliverable Title	Author or Organisation	Type
1	AC/DC parallelised and tested code running on NESSC supercomputer	Itasca	Software code
2	A Summary of the State of the AC/DC Package, and its Current Capabilities	P. Cundall, Itasca, February 2003	Report
3	AC/DC visualization and analysis software	Liverpool University	Software code
4	AC/DC Visualizer (ACDCVIS) Deliverable Report on Key Features and Capabilities	A. Heath, D. Collins, J. Hazzard, P. Young, Liverpool University, February 2003	Report
5	Static Behavior of Best-fit PFC Materials for Lac du Bonnet Granite	D. Potyondy, F. Dedecker, Itasca, March 2003	Report/ Methodology
6	PFC Stress Corrosion Model	D. Potyondy, Itasca, March 2003	Report/ Methodology
7	Laboratory and PFC3D Elastic Constant and Wave Velocity Comparisons	D. Potyondy, Itasca, October 2003	Report/ Methodology and Data Set
8	Modelling Seismicity in PFC3D	J. Hazzard, Liverpool University August 2002	Report/ Methodology
9	Modelling of Acoustic Emissions	J. Hazzard, D. Collins, Liverpool University, April 2003	Report/ Methodology and Data Set
10	Laboratory Tests to Investigate the Static and Dynamic Elastic Moduli of Crosland Hill Sandstone	C. Baker, W. Pettitt, ASC Ltd, October 2003	Report and Data Set
11	Acoustic Emission Observations of Rock Fracture under True-triaxial Stress	W. Pettitt, J. Haycox, ASC Ltd, October 2003	Report and Data Set
13	Static Excavation Study in AC/DC (Aspo Diorite)	F. Dedecker, D. Billaux, Itasca, October 2004	Report/ Methodology and Data Set
14	Dynamic Modelling Studies Using AC/DC	J. Hazzard, D. Collins, Liverpool University, August 2004	Report/Methodology and Data Set
15	Acoustic Emission and Ultrasonic Monitoring of Deposition Hole DA3545G01 During the Excavation and Heating Phases	W. Pettitt, J. Haycox, ASC Ltd, July 2004	Report and Data Set
16	AC/DC Modelling of the Excavation in the Callovo Oxfordian Argillite	F. Dedecker, D. Billaux, Itasca, October 2004	Report and Data Set
17	AC/DC Modelling of Mont Terri Clay Excavation	F. Dedecker, D. Billaux, Itasca, October 2004	Report and Data Set
18	Comparison of Modelled and Measured Static and Dynamic Moduli from the Imperial College Polyaxial Experiment	D. Potyondy, Itasca; J. Hazzard, Liverpool, October 2004	Report and Data Set

**Table 3: The reports and datasets associated with the deliverables for the project.**

## 8 APPENDIX 2 — EXPLOITATION AND DISSEMINATION

A Technology Implementation Plan (TIP) was submitted to the EU with this Final Technical Report. In summary, Table 4 presents the main project results for SAFETI.

Main Project Result	Description	Ownership
1. Modelling Software	A software program called AC/DC for modelling 3D rock behaviour on a parallel-computing facility.	Itasca
2. Visualization Software	A software program (ACDCvis) for visualizing and analyzing the results in 3D from AC/DC models and seismic data sets.	Liverpool University
3. Laboratory seismic data set	A processed data set of rock properties, acoustic emission (AE) parameters, seismic velocities, and elastic stiffness values, from laboratory rock samples (Crosland Hill sandstone) undergoing specific polyaxial loading experiments.	ASC
4. Procedure for PFC3D modelling of rock	A calibrated procedure for producing a PFC3D ‘model of rock’ that matches the static behaviour of laboratory rock samples under certain loading conditions.	Itasca
5. Algorithms for PFC3D seismic modelling	A set of calibrated algorithms for modelling the dynamic (seismic) behaviour of laboratory rock samples under certain loading conditions using PFC3D.	Liverpool University
6. Insitu seismic data set	A processed data set of rock properties, AE parameters, seismic velocities, and elastic stiffness values, from the SKB PRT excavation study.	ASC
7. Procedure for AC/DC modelling of field scale studies.	A validated procedure/methodology for modelling the static and dynamic behaviour of rock in field scale studies for both short and long time periods using AC/DC.	Liverpool/Itasca

**Table 4: The main project results from SAFETI.**

The intellectual property rights (IPR) and ownership of each of the 7 results will rest with the individual partners that developed each result as indicated in Table 4. The AC/DC code is owned by Itasca and it is likely that it will be developed by Itasca in the future. The AC/DC software can be purchased from Itasca by contacting them by phone or through their website. Itasca are also likely to benefit from AC/DC through their consulting activities, and taught courses. The ACDCvis code is owned by the University of Liverpool, but an agreement has been made for Itasca or ASC to further develop the codes (non exclusive licence). All of the partners that have developed results will market them through publications and conferences, which make the results unpatentable, and enforce by law ownership of a result to that partner. A number of the methods and results have already been published.

The main dissemination of the results by the partners will be in the form of journal publications, presentations at international conferences, and conference proceedings. Marketing of the AC/DC modelling code and methods as well as controlled seismic (AE) monitoring methods, will be an important activity of the Industry partners Itasca and ASC, through their websites and brochures.

The initial targeted audience is scientists, researchers, and engineers in the fields of radioactive waste disposal, earth sciences, mining and civil engineering. Table 5 lists 11 of the biggest nuclear waste management agencies in the EU. The AC/DC codes and methods will be of interest to a number of universities and dedicated research institutes. There are currently 100’s of PFC3D users Worldwide, who are likely to be interested in the increased possibilities and major

advance in the size of 3D models that can be simulated with AC/DC. The results will also be used to market the University of Liverpool to help attract promising graduate students, post-doctoral researchers and further research funding.

AC/DC will be of interest to a broad engineering sector, since it can be used to model the effects of stress on any brittle material including rock and concrete. The AC/DC methodology could be applied for example, to concrete structures such as dams, particularly for understanding their long-term stability due to material degradation. AC/DC will be of interest to petroleum companies to model the effect of reservoir property change with time. Microseismic monitoring has recently become an important tool of petroleum companies for determining the extent of fracture networks during oil extraction or following hydraulic fracturing techniques. This type of data would be very complementary with AC/DC for model validation. AC/DC will also be of interest to Earth Science and geology survey companies, due to the relevance to stress effects on the Earth's crust such as earthquakes and subduction zones. In the short and long term, the results of this project are expected to lead to jobs in a broad range of engineering activities.

<i>Country</i>	<i>Radioactive Waste Management Agency</i>
Belgium	ONDRAF/NIRAS
Czech Republic	SURAO (RAWRA)
Finland	POSIVA
France	ANDRA
Germany	BfS
Hungary	PURAM
Italy	NUCLECO
The Netherlands	COVRA
Spain	ENRESA
Sweden	SKB
United Kingdom	NIREX, BNFL, UKAEA

**Table 5: The initial waste management target market.**

The following papers have been presented, or published:

- Dedecker, F., and D. Billiaux, 2005. Evaluation of Damage-induced Permeability in the Bure Site using a Three Dimensional Adaptive Continuum / Discontinuum Code, in Proceedings of the International Symposium hosted by ANDRA 'Using Natural and Engineering Clay-based Barriers for the Containment of Radioactive Waste', March, Tours.
- Young, R.P., Collins, D.S., Pettitt, W. S., and Hazzard, J. F., 2004. Imaging and Visualization of Fractures in Rock Engineering, in *Proceedings of the 3<sup>rd</sup> ARMS*, Kyoto, Japan, pp10.
- Billiaux, D., Dedecker, F., and Cundall, P., 2004. A Novel Approach to Studying Rock Damage: The Three Dimensional Adaptive Continuum / Discontinuum Code, in *'Rock Engineering: Theory and Practice'*, in *Proceedings of the ISRM Regional Symposium EUROCK & 53<sup>rd</sup> Geomechanics Colloquy*, Salzburg, Editor W. Schubert, pp 723-728.
- Hazzard, J.F. and R.P. Young, 2004. Numerical investigation of induced cracking and seismic velocity changes in brittle rock, *Geophysical Research Letters*, 31, L01604, doi:10.1029/2003GL019190.
- Potyondy, D. and Cundall, P., 2004. A bonded-particle model for rock, *International Journal of Rock Mechanics & Mining Sciences*, 41, 8, 1329-1364.
- Hazzard, J.F. and R.P. Young, 2004. Dynamic modelling of induced seismicity, *International Journal of Rock Mechanics & Mining Sciences*, 41, 8, 1365-1376.
- Young, R.P., Collins, D.S., Hazzard, J., Heath, A., Pettitt, W.S., Baker, C., Billiaux, D., Cundall, P., Potyondy, D., Dedecker, F., Svemar, C., and Lebon, P., 2004. An Innovative 3-D Numerical Modelling Procedure for Simulating Repository-Scale Excavations in Rock – SAFETI, in

*Proceedings of the Euradwaste '04 Conference on Radioactive Waste Management Community Policy and Research Initiatives*, Luxembourg, pp5.

- Young, R.P., Collins, D.S., Hazzard, J., Heath, A., Baker, C., Pettitt, W.S., Billaux, D., Cundall, P., Potyondy, D., Dedecker, F., & Svemar, C., 2003. An Innovative 3-D Numerical Modelling Procedure for Simulating Repository-Scale Excavations in Rock – SAFETI, in *Proceedings of the CLUSTER Conference on Impact of the EDZ on the performance of radioactive waste geological repositories*, Luxembourg, pp5.
- Hazzard, J.F. and Young, R.P., 2002. 3D Numerical Modelling of Acoustic Emissions, presented at the 5<sup>th</sup> International Workshop on the Application of Geophysics in Rock Engineering, as part of the 5<sup>th</sup> North American Rock Mechanics Symposium, July 2002. (The paper is available at: <http://www.liv.ac.uk/seismic/news/narms/narms.html>).

Topics of future papers and presentations include:

- Static and dynamic modulus changes during true triaxial loading of a sandstone cube. Part 1: Laboratory studies, Part 2: Numerical modelling
- A programme for 3D visualisation of mechanical and seismic data in rock mechanics
- An adaptive continuum/discontinuum numerical modelling technique for efficient 3D simulation of inelastic rock masses
- Cracking and failure around heated excavations in brittle rock. Part 1: Acoustic results, Part 2., Numerical modelling
- Simulating stress corrosion with a bonded-particle model for rock

## 9 APPENDIX 3 — CONTACT DETAILS CONCERNING FOLLOW-UP OF THE PROJECT

The main participants in the project are shown in Table 6.

PARTNER	NAME
<u>University of Liverpool</u> Dept of Earth Sciences, 4 Brownlow Street, Liverpool, L69 3GP, England +44 (0) 151 794 5160 ( <a href="http://www.liv.ac.uk/seismic">www.liv.ac.uk/seismic</a> ).	Prof. R.P. Young (Project co-ordinator) Dr. D. Collins Dr. J. Hazzard Dr. A. Heath Mr. A. McCormack
<u>Applied Seismology Consultants Ltd</u> 5 Swan Hill Court, Shrewsbury, SY1 1NP, England. +44 (0) 1743 271440 ( <a href="http://www.appliedseismology.com">www.appliedseismology.com</a> )	Dr. W. Pettitt Dr. C. Baker Mr. J. Haycox
<u>Itasca Consulting Group, S.A.</u> 64 Chemin des Mouilles, 69130 Ecully, France +33 472180420 ( <a href="http://www.itasca.fr">www.itasca.fr</a> ).	Dr. D. Billaux Dr. P. Cundall Dr. D. Potyondy Dr. F. Dedecker
<u>SKB</u> Aspolaboratoriet, PL 300, SE-572 95, Figeholm, Sweden ( <a href="http://www.skb.se">www.skb.se</a> ).	Mr C. Svemar
<u>ANDRA</u> Parc de la Croix Blanche, 1/7 rue Jean Monnet, 92298 Chatenay-Malabry Cedex, France ( <a href="http://www.andra.fr">www.andra.fr</a> ).	Mr P. Lebon Dr N. Hoteit

**Table 6: The main participants in the SAFETI project and the associated contact details. Note: At the date of this report, the contact details for R. P. Young are: University of Toronto, 35 St. George St., Toronto, M5S 1A4, Canada, +1 416 978 5252; Email: [paul.young@utoronto.ca](mailto:paul.young@utoronto.ca); Website: [www.lassondeinstitute.utoronto.ca/young](http://www.lassondeinstitute.utoronto.ca/young).**

A webpage for SAFETI was produced at: [www.liv.ac.uk/seismic/research/current/safeti.html](http://www.liv.ac.uk/seismic/research/current/safeti.html). The project summary is also contained and updated by ASC on: [www.appliedseismology.com/newsitem.aspx?newsid=2](http://www.appliedseismology.com/newsitem.aspx?newsid=2).